Journal of African Earth Sciences 238 (2026) 106106

Contents lists available at ScienceDirect

Journal of African Earth Sciences

journal homepage: www.elsevier.com/locate/jafrearsci

Geochemical and Sr-Nd isotope constraints on the provenance of Permian deposits from Mozambique's Lower Karoo Zambezi Basin

R.C.G.S. Jorge [a,*], P. Fernandes [b], Z. Pereira [c], J.F. Santos [d], G. Lopes [e], J. Marques [f]

[a] Universidade de Lisboa, Faculdade de Ciências, Instituto Dom Luiz, Campo Grande, Edifício C6, Piso 4, 1749-016, Lisboa, Portugal
[b] CIMA – Centre of Marine and Environmental Research\\ARNET - Infrastructure Network in Aquatic Research, University of Algarve, Campus de Gambelas, 8005-139, Faro, Portugal
[c] Laboratório Nacional de Energia e Geologia (LNEG), Rua da Amieira, 1089, S. Mamede Infesta, Apartado, 4466-901, Portugal
[d] GeoBioTec, Department of Geosciences, University of Aveiro, 3810-193, Aveiro, Portugal
[e] Plants, Photosynthesis and Soil, School of Biosciences, University of Sheffield, Western Bank, Sheffield, S10 2TN, UK
[f] Gondwana Empreendimentos e Consultorias, Limitada, Rua 1.335, no. 233, Bairro da COOP, Caixa Postal 832, Maputo, Mozambique

ARTICLE INFO

Handling Editor: M Mapeo

Keywords:
Geochemistry
Palaeogeography
Palaeoweathering history
Moatize
Minjova sub-basin
Moatize formation
Matinde formation

ABSTRACT

Whole-rock geochemistry and Sr-Nd isotopic compositions of Permian mudrocks from the Moatize and Matinde formations were analysed to constrain the sediment provenance, weathering history and palaeogeographic setting of the Moatize - Minjova Sub-Basin in the Karoo Zambezi Basin of Mozambique. The geochemical signatures of both formations suggest minimal effects of recycling and sorting, and point to rapid sediment deposition within an active tectonic setting. Trace element systematics and key provenance ratios (Th/Sc, La/Sc, Cr/Th, La_N/Sm_N, Eu/Eu*) indicate heterogeneous source areas dominated by felsic rocks with a minor mafic contribution. The mudrocks of the Moatize and Matinde formations exhibit similar isotopic signatures, with εNd (t) values of −9.32 ± 0.74 and −7.99 ± 1.10, and Nd T_{DM} model ages of 1.68 ± 0.08 and 1.51 ± 0.12 Ga, respectively. These isotopic signatures indicate that both formations were derived from mixed sources, including late Mesoproterozoic and Neoproterozoic rocks from southern Malawi, the Nampula Block (a subdomain of southernmost Malawi), the Guro Suite and the Macossa-Chimoio Nappe.

Both Moatize and Matinde mudrocks exhibit high Chemical Index of Alteration (>85) and Chemical Index of Weathering (>90) values, along with low Index of Compositional Variability and low K/Cs ratios. The Al_2O_3–(CaO + Na_2O)–K_2O (A–CN–K) relationships indicate that the Moatize and Matinde mudrocks have not undergone post-depositional K-metasomatism. The data collectively indicate intense palaeoweathering conditions in the source areas. Furthermore, the weathering indices suggest warm and humid palaeoclimate during the deposition of the Moatize and Matinde formations. These formations were deposited in a confined continental basin between the Guadalupian (middle Permian) and the Lopingian (late Permian).

1. Introduction

During the Pangaea times (Late Carboniferous to Early Jurassic), Africa occupied the core of the Gondwana supercontinent (Torsvik and Cocks, 2017; Gradstein et al., 2020). This period was marked by important geological, biological, and climatic events that profoundly affected Gondwana. Among the most extensively studied is the drastic shift from the icehouse conditions of the Late Palaeozoic glaciations to the hothouse conditions that prevailed throughout the Triassic, accompanied by widespread aridity (*e.g.,* Retallack, 2013). All these events are recorded in the Gondwanan rock record, particularly within the sedimentary sequences of the African Karoo basins (Catuneanu et al., 2005; Hancox, 2016; Götz et al., 2020).

These basins comprise the Main Karoo Basin (MKB) in South Africa, and a network of continental rift basins to its north of the MKB. The MKB is a foreland basin bounded to the south by the mountains of the Cape Fold Belt (*e.g.,* Catuneanu et al., 2005; Viglietti et al., 2017). The continental rift basins formed through the reactivation of high-strain shear zones (Fig. 1a), which were inherited from Precambrian to early Cambrian tectonics (*e.g.,* Afonso, 1984; Delvaux, 2001;

* Corresponding author.
E-mail addresses: rjorge@fc.ul.pt (R.C.G.S. Jorge), pfernandes@ualg.pt (P. Fernandes), zelia.pereira@lneg.pt (Z. Pereira), jfsantos@ua.pt (J.F. Santos), gilda.lopes.geo@gmail.com (G. Lopes), joaomarques@gondwana.co.mz (J. Marques).

https://doi.org/10.1016/j.jafrearsci.2026.106106
Received 12 May 2024; Received in revised form 24 February 2026; Accepted 25 February 2026
Available online 26 February 2026

GTK-Consortium, 2006). Consequently, studies have shown that the African Karoo basins differ not only in their tectonic style, but they also in their stratigraphic sequences and palynological records (*e.g.,* Nyambe and Dixon, 2000; Catuneanu et al., 2005; Jacobs et al., 2005; Isbell et al., 2008; Phiri et al., 2016; Barbolini et al., 2018). The sedimentary records of the MKB indicate a transition from predominantly marine environments in the Late Carboniferous – Early Lopingian) to mainly non-marine environments by the Middle Guadalupian – Middle Jurassic (*e.g.,* Smith, 1990; Johnson et al., 1996; Rubidge and Day, 2020; Baiyegunhi and Liu, 2021; Bordy and Paiva, 2021). By contrast, sedimentation in the rift basins occurred largely in non-marine settings (Johnson et al., 1996; Catuneanu et al., 2005; Hancox, 2016).

This study focuses on the Moatize-Minjova Sub-Basin (MMSB) (Fig. 1b and 2), which forms part of the larger Karoo Zambezi Basin of Mozambique (KZBM). This basin is also a component of the network of continental Karoo rift basins across sub-Saharan Africa (Fernandes et al., 2023, 2024). The MMSB is primarily known for its extensive coal deposits, particularly within the Moatize Coalfield (Real, 1966; Afonso, 1984; Vasconcelos, 1995; Vasconcelos and Achimo, 2010).

The MMSB has recently been studied in detail in terms of stratigraphy and depositional settings (Bicca et al., 2017; Lopes et al., 2021; Fernandes et al., 2023), palynology (Pereira et al., 2016, 2019; Galasso et al., 2019), detrital zircon U-Pb geochronology (Bicca et al., 2018; Fernandes et al., 2024), and tectonics and thermal history (Fernandes et al., 2015, 2023, 2024; Bicca et al., 2017; Galasso et al., 2019). Despite these advances in the geological understanding of the MMSB, the geochemistry of its sedimentary successions remains poorly understood, with no published studies to date. This study addresses this gap in geological knowledge by presenting and discussing, for the first time, whole-rock geochemical data including major, trace, and rare earth elements, as well as Sr-Nd isotopic compositions for mudrocks of the Lower Karoo Group in the MMSB. These data provide new insights into the interval between the end of the Late Palaeozoic glaciation and the Late Permian coal-forming environments. This study also evaluates the palaeoweathering conditions during this depositional interval, the variability in source area composition, and the potential effects of sedimentary recycling. These original data are further used to constrain the paleoclimatic and palaeoenvironmental settings of the MMSB in the broader context of the evolution of the Karoo basins of Gondwana.

2. Geological setting

The Lower Karoo Group is well represented in the KZBM in Tete Province (Fig. 1b and 2). This stratigraphic unit was deposited in intracratonic graben and half-graben-type sedimentary basins that developed along the strike of pre-existing high-strain geological sutures formed during the Pan-African Orogeny (620 - 530 Ma) (GTK-Consortium, 2006; Norconsult Consortium, 2007; Viola et al., 2008). The crystalline basement of Tete Province, upon which the KZBM developed, consists of collage of different Gondwana terranes (*e.g.,* GTK-Consortium, 2006; Grantham et al., 2008; Macey et al., 2010; Fritz et al., 2013; Thomas et al., 2022). The East and West Gondwana terranes

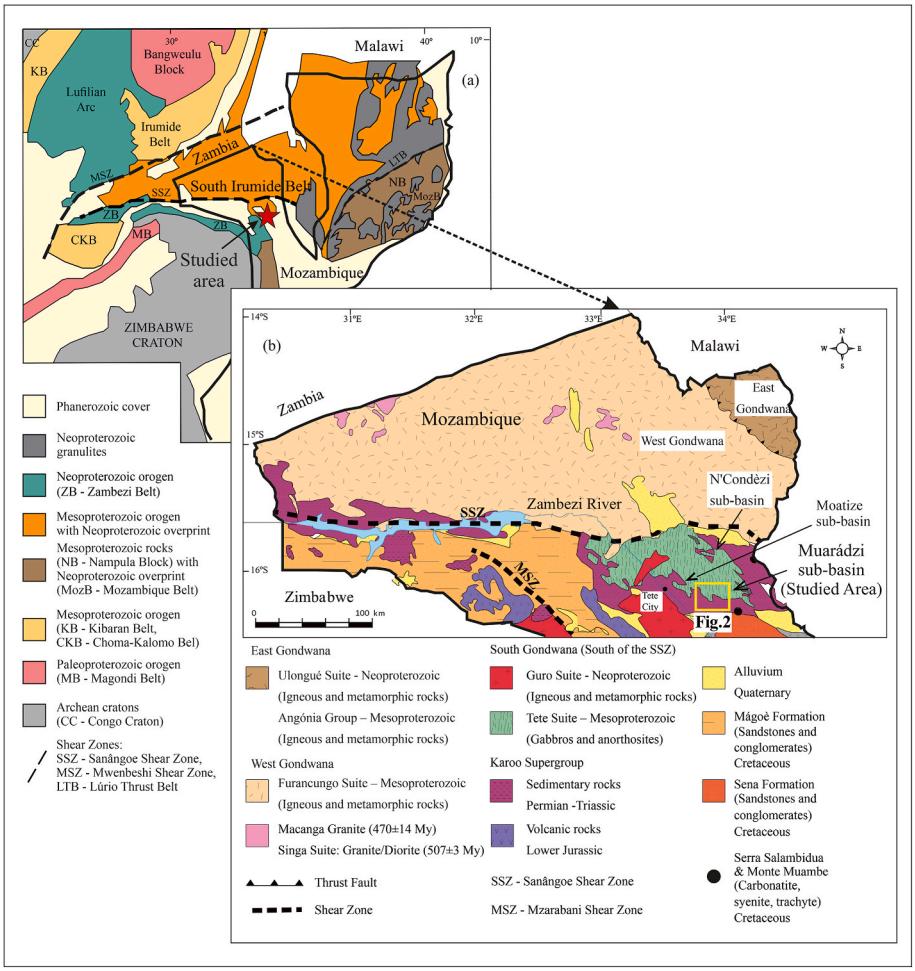

Fig. 1. (a) Crustal age domains and tectonic framework of the studied region. Adapted from Chaúque et al. (2017). (b) Simplified geology of the Province of Tete, Mozambique, showing the location of the Karoo rocks and basins. Adapted from Carta Geológica República de Moçambique, Escala 1/1,000,000 (2008) and Galasso et al. (2019). (For interpretation of the references to colour in this figure legend, the reader is referred to the Web version of this article.)

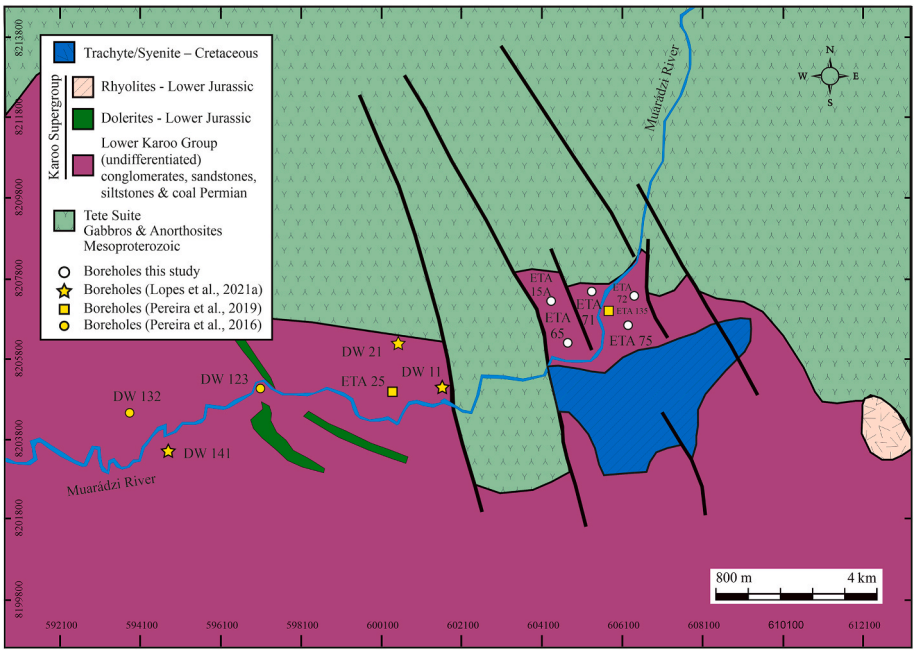

Fig. 2. Detailed geology of the studied region with the location of the boreholes investigated and the location of other boreholes mentioned in this work. Adapted from Geological Map of Mozambique, sheet no. 1633, Tete, Geological Series 1/250,000, Direcção Nacional de Geologia, Maputo (2006). (For interpretation of the references to colour in this figure legend, the reader is referred to the Web version of this article.)

comprise Mesoproterozoic granites and gneisses of the Southern Irumide Belt (1060 – 950 Ma; Fritz et al., 2013), one of several orogenic belts responsible for the assembly of the Supercontinent Rodinia (ca. 1000 Ma; GTK-Consortium, 2006; Norconsult-Consortium, 2007). The Mesoproterozoic rocks of the Furancungo Suite (West Gondwana) and the Angónia Group (East Gondwana) were later reworked during the late Neoproterozoic - Cambrian orogeny, which also led to the intrusion of granite batholiths (GTK-Consortium, 2006; Norconsult-Consortium, 2007).

The Cambrian-Ordovician Singa (507 Ma) and Macanga (470 Ma) granites intruded the West Gondwana terrane, whereas the Neoproterozoic Ulônguè Suite (575 - 545 Ma) intruded the East Gondwana terrane (GTK-Consortium, 2006; Norconsult-Consortium, 2007). In northeastern Mozambique, the WSW-ENE trending Lúrio Belt separates the Marrupa-Unango and Cabo Delgado Nappe Complex to north from the Nampula Block to the south (Fritz et al., 2013, Fig. 1b).

The Nampula Block is a continuous late Mesoproterozoic crustal block covering more than 100,000 km^2, mainly composed of high-grade metamorphic orthogneisses and metasedimentary rocks (Macey et al., 2013). It is tectonically overlain by allochthonous Neoproterozoic granulites of the Monapo-Mugeda Klippen and by para-autochthonous (meta)sediments of the Mecubúri and Alto Benfica groups (Macey et al., 2013).

The South Gondwana terrane is characterised by Mesoproterozoic gabbros and anorthosites of the Tete Suite, as well as the Neoproterozoic igneous and metamorphic rocks of the Guro Suite (867 Ma) (GTK-Consortium, 2006; Norconsult-Consortium, 2007, Fig. 1b).

The Zimbabwe Craton is exposed south of the KZBM (Fig. 1a). The Macossa-Chimoio and Mungari nappe complexes are tectonically juxtaposed against the Zimbabwe Craton. Chaúque et al. (2017, 2019) proposed that the Nampula Block can be correlates with the Macossa-Chimoio Nappe. This nappe comprises high-grade paragneisses, granulites and migmatites that form the Macossa and Chimoio groups (1000 – 1200 Ma). Both groups are closely associated with the Mesoproterozoic granitoid rocks of the Báruè Complex (Chaúque et al., 2019).

The Karoo sedimentary cycle in Mozambique, which occurred from the Late Cisuralian (lower Permian) to the Early Jurassic, corresponds to the infill of several intracratonic extensional basins. Post-Karoo faulting associated with the breakup of Gondwana and the onset of rifting in the western Indian Ocean led to segmentation of the initial depocenters into the three sub-basins recognised today, from west to east: Chicôa-Mecúcoè, Sanângoè-Mefidéze, and Moatize-Minjova (Afonso and Marques, 1993; Afonso et al., 1998; Hartzer et al., 2008). These sub-basins share a similar Lower Karoo Group stratigraphic succession containing workable coal seams (Vasconcelos and Achimo, 2010; Hancox, 2016). According to the terminology used by coal exploration companies that operated in the MMSB, this basin was further subdivided into three coalfields: Moatize, Muarádzi, and N'Condédzi (*e.g.,* GTK-Consortium, 2006; Norconsult-Consortium, 2007, Figs. 1b and 2).

The Lower Karoo Group in the MMSB comprises three clastic formations (listed from oldest to youngest): the Vúzi, Moatize, and Matinde formations (*e.g.,* GTK-Consortium, 2006; Norconsult-Consortium, 2007, Fig. 3). The Vúzi Formation unconformably overlies the Precambrian basement rocks and consists of matrix to clast-supported conglomerates interbedded with sandstones, siltstones and mudstones. The thickness of this formation varies, and the sequence is interpreted as the result of fluvioglacial and lacustrine processes (Achimo et al., 2014; Fernandes et al., 2023). The age of the Vúzi Formation remains debated, although it is most probably Kungurian to early Roadian (Lopes et al., 2021a; Fernandes et al., 2023).

The Moatize Formation lies conformably on the Vúzi Formation or unconformably on the Precambrian basement rocks. Its type area is defined in the Moatize Coalfield, where it comprises a 340 m thick succession of interbedded sandstones, siltstones, carbonaceous mudstones, and six principal coal seams. The Moatize Formation is interpreted as having been deposited in lacustrine and fluvial settings (GTK-Consortium, 2006; Fernandes et al., 2023). The sandstones represent channel-fill deposits of braided and meandering rivers, whereas the mudstones and siltstones indicate swamp-like overbank environments or deposition on lake floors and along lake margins (*e.g.,* Real, 1966; Vasconcelos, 1995; GTK-Consortium, 2006; Fernandes et al., 2023). The age of the Moatize Formation was recently reassessed by Lopes et al. (2021a) and Fernandes et al. (2023), who concluded that the most probable age for its base is early Roadian. In contrast, the upper boundary with the overlying Matinde Formation is diachronous, ranging

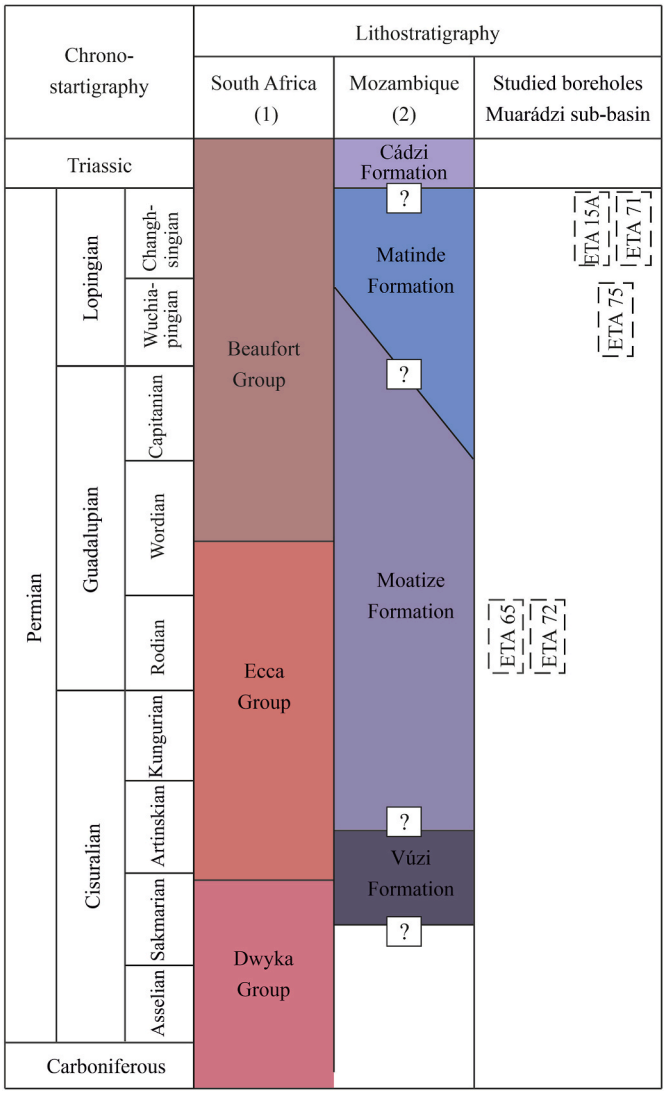

Fig. 3. Lithostratigraphic scheme for the Moatize-Minjova Coal Basin and its correlation with the Main Karoo Basin of South Africa, showing the stratigraphic positions of the boreholes studied. After Lopes et al. (2021b). (For interpretation of the references to colour in this figure legend, the reader is referred to the Web version of this article.)

from early Capitanian to late Wuchiapingian (Lopes et al., 2021a; Fernandes et al., 2023).

The Matinde Formation rests conformably on the Moatize Formation and is composed of interbedded coarse-to fine-grained sandstones, siltstones, and carbonaceous mudstones, with coal beds intercalated throughout. Conglomerate beds are relatively uncommon (*e.g.,* Real, 1966; Vasconcelos, 1995; GTK-Consortium, 2006). Pereira et al. (2016. 2019) described conglomerates interbedded within the Matinde Formation in the Muarádzi Coalfield. The sandstone beds exhibit sedimentary features typical of fluvial channel-fill deposits, while the siltstones, mudstones and interbedded coal seams are interpreted as fluvial overbank deposits (Bicca et al., 2017; Lopes et al., 2021b; Fernandes et al., 2023). The thickness of the Matinde Formation is approximately 2 km in the MMSB (GTK-Consortium, 2006; Pereira et al., 2019). Fernandes et al. (2023) proposed that tectonic activity was the primary allogenic factor controlling the deposition of the Moatize and Matinde formations. According to these authors, the initial tectonism that shifted the sedimentary environments from lake-delta to bedload (braided) rivers took place within the upper part of the Moatize Formation. A new braided river belt emerged during a second tectonic pulse, which established the boundary between the Moatize and Matinde formations. The base of the Matinde Formation is diachronous, as described above, and its upper part may coincide with the Permo-Triassic boundary (Pereira et al., 2016; Galasso et al., 2019).

3. Materials and methods

3.1. Sampling and borehole descriptions

Bulk mineralogical, geochemical and Sr-Nd isotopic data were obtained from the study and sampling of five coal exploration boreholes (ETA 15A, ETA 65, ETA 71, ETA 72, and ETA 75) drilled in the Muarádzi Coalfield of the MMSB. Their geographic distribution is show in Fig. 2. Samples were collected systematically along the boreholes, excluding coals seams and the most organic-rich intervals (Fig. 4), as well as intervals affected by post-depositional alterations or recent weathering.

The sequence observed in all studied boreholes consists of black carbonaceous mudstones with thin coal beds, black to grey mudstones, siltstones, sandstones, and conglomerates (Fig. 4). The mudrock lithologies show frequent plant imprints, while the sandstones exhibit normal grading with current related sedimentary structures such as cross-lamination and cross-bedding. Conglomerates occur in all five boreholes and are matrix-supported and poorly sorted, with clast sizes ranging from granule to pebble (Fig. 5). The matrix of these conglomerates is mainly silt to fine-grained sand.

The successions of boreholes ETA 65 and ETA 72 were assigned to

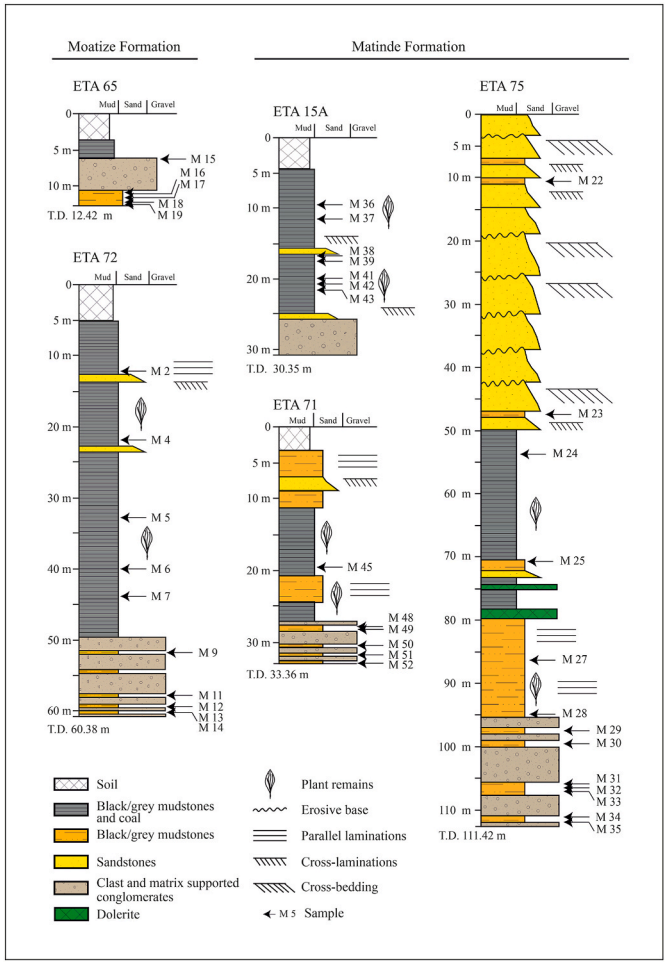

Fig. 4. Lithological logs of the studied boreholes, indicating the locations of the analysed samples. (For interpretation of the references to colour in this figure legend, the reader is referred to the Web version of this article.)

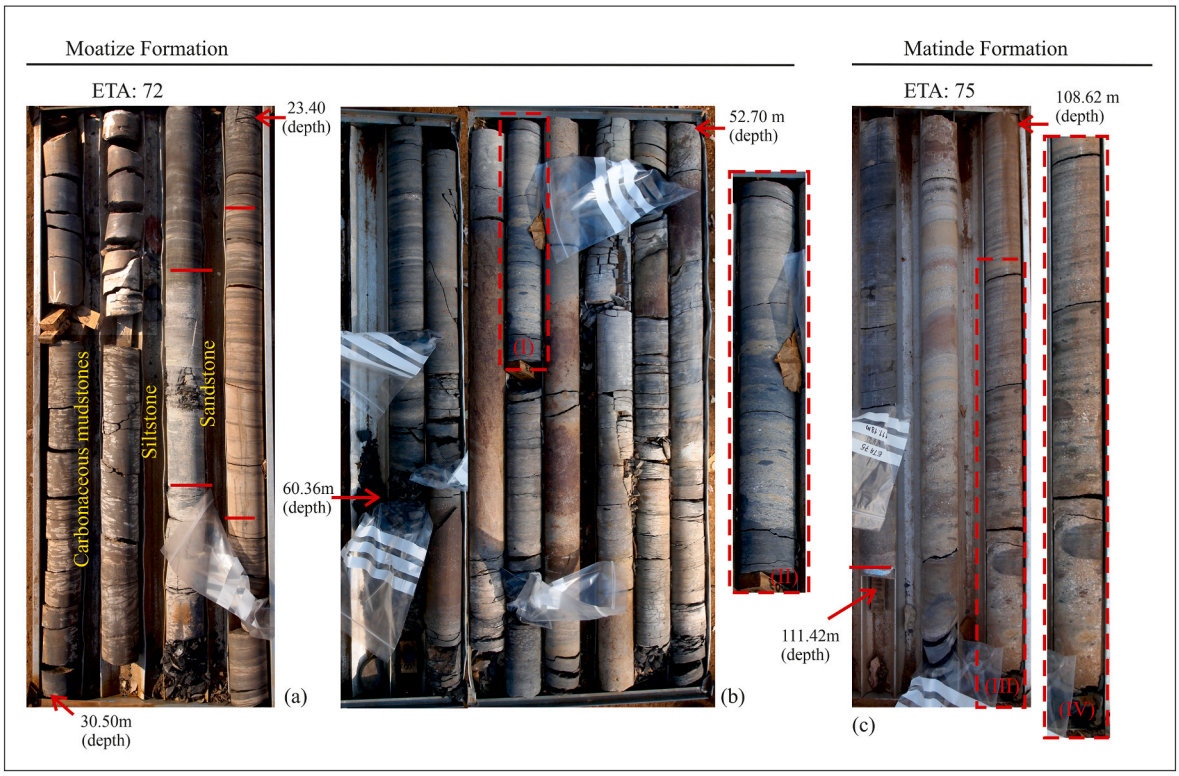

Fig. 5. (a) Core interval of borehole ETA 72 between 30.5 m and 23.2 m depth, displaying typical carbonaceous mudstones with thin coal beds interbedded with siltstones and fine-grained sandstones with cross-laminations. The thin coal beds are absent from the core because they were sampled for coal analysis before our sampling. (b) Core interval of borehole ETA 72 between 60.38 m and 52.7 m depth. *Box*I is enlarged in box II, showing the sedimentary features of the conglomerates at the base of this borehole, including erosive base, normal grading, clast-to-matrix-supported fabric, and mud clast. (c) Core interval of borehole ETA 75 between 111.42 m and 108.62 m depth. Box III is enlarged in box IV, highlighting the features of the conglomerates at the base of this borehole. (For interpretation of the references to colour in this figure legend, the reader is referred to the Web version of this article.)

the lower part of the Moatize Formation and yielded palynomorph assemblages indicating an early Cisuralian age (Lopes et al., 2014; Pereira et al., 2014). In contrast, boreholes ETA 15A, ETA 71 and ETA 75 yielded palynomorphs assigned to the Lopingian (upper Permian) (Costa et al., 2016; Pereira et al. (2019), an age that characterises the Matinde Formation (Lopes et al., 2021a; Fernandes et al., 2023).

3.2. Methods

Whole-rock X-ray diffraction (XRD) analyses were conducted on 7 mudstones (M2, M4, M10, M12, M14, M16 and M17) from the Moatize Formation and 8 mudstones (M22, M27, M28, M32, M36, M41, M48, M50 and M52; Fig. 4) from the Matinde Formation. Analyses were conducted at the Laboratory of Mineralogy and Petrology from the Center for Natural Resources and Environment (IST - University of Lisbon) using a PANalytical X'PERT PRO diffractometer with CuKα radiation. Measurement conditions were a 2θ range of 5–70°, a step size of 0.033°, and scan time of 80 s per step. The X-ray generator operated at 40 kV and 35 mA. Data were analysed using X'PERT PLUS software and the PDF4 database.

Forty-one representative mudstones, 15 from the Moatize Formation and 26 from the Matinde Formation, were selected for whole-rock geochemical analysis (Fig. 4). Samples were crushed o chips and powdered in an agate mill. Major elements plus Ba and Sr were analysed by inductively coupled plasma-optical emission spectrometry (ICP-OES), and most trace elements by inductively coupled plasma-mass spectrometry (ICP-MS). Analyses were performed at Activation Laboratories Ltd. (ACTLABS, Ontario, Canada; Codes 4- Lithoresearch and 4B-INAA), using standard procedures for each method. Alkaline dissolution with lithium metaborate/tetraborate, (followed by nitric acid dissolution), was performed for all analyses, except for the determination of Cu, Ni, and Zn, for which acid digestion was carried out. Standards included GXR-1, NIST 694, DNC-1, GBW 07113, GXR-4, SDC-1, GXR-6, LKSD-3, SY-4, CTA-AC-1, BIR-1a, NCS DC86312, NCS DC70014, SAR-M (USGS), and OREAS 100a (Fusion). Analytical reproducibility is better than 3% for major elements, less than 4% for rare earth elements (REE), and ≈5% for HFSE. Further details on analytical procedures are available at http://www.actlabs.com, and the complete geochemical dataset is provided in Electronic Appendix A.

Six representative mudstones, 4 from the Moatize Formation and 2 from the Matinde Formation, were selected for whole-rock Sr and Nd isotope analysis (Fig. 4). Isotopic compositions of mudstones were determined by thermal ionization mass spectrometry (TIMS) under ultra–clean conditions at the Laboratory of Isotopic Geology, University of Aveiro (LGI-UA, Portugal). The dissolved samples were processed by two-stage cation exchange chromatography: (1) Sr and the REE fractions were separated in two overlapping columns containing Sr-resin (50-100 μm), and TRU-resin (50-100 μm), both resins from Triskem International; (2) Nd was separated from other lanthanides in columns containing cation exchange Ln-resin from Eichrom. Strontium was loaded onto a single Ta filament with H_3PO_4, and Nd on a Ta outer side filament with HCl in a triple filament arrangement.

The $^{87}Sr/^{86}Sr$ and $^{143}Nd/^{144}Nd$ i ratios were measured on using a multi-collector Thermal Ionization Mass Spectrometer (TIMS) VG Sector 54 in dynamic mode with peak intensities of 1–2 V for ^{88}Sr and 0.5–1.0 V for ^{144}Nd. Repeated analyses of the SRM 987 and JNdi-1 standards provided, mean values of $^{87}Sr/^{86}Sr = 0.7102627 \pm 23$ (95% confident limit; $n = 14$) and $^{143}Nd/^{144}Nd = 0.512084 \pm 15$ (95% confidence limit; $n = 13$). Analytical errors are reported throughout as 2σ.

3.3. Geochemical indices

In this study, Chemical Index of Alteration (CIA; Nesbitt and Young, 1982) and the Chemical Index of Weathering (CIW; Harnois, 1988) were applied to infer palaeoweathering conditions in the source area of the Moatize and Matinde formations. The indices are calculated as CIA = $[Al_2O_3/(Al_2O_3 + CaO^* + Na_2O + K_2O)] \times 100$; and CIW = $[Al_2O_3/(Al_2O_3 + CaO^* + Na_2O)]$ x 100; all expressed in molar proportion and CaO* representing CaO incorporated in silicates. CIA values of unweathered plagioclase and K-feldspar are approximately 50, whereas those for kaolinite and chlorite approach ~100. CIA values increase with the degree of weathering.

The Index of Compositional Variability (ICV; Cox et al., 1995) is used to evaluate mudstone compoitional maturity and is calculated as $[(Fe_2O_3 + K_2O + CaO + MgO + TiO_2)/Al_2O_3]$; with oxides in weight percent. The ICV values decrease with increasing maturity of mudstones. Both CIW and ICV are less affected by diageneses such as post-depositional K-addition (*e.g.,* Harnois, 1988).

4. Results

4.1. Mineralogy

XRD analysis reveals that the clay mineral assemblage of the Moatize Formation is highly homogeneous and dominated by kaolinite, with minor muscovite and subordinate mixed-layer illite/mica. The mudrocks of the Moatize Formation display a similar clay mineral assemblage. In both formations, the non-clay minerals are predominantly quartz (Fig. 6).

4.2. Major elements

The average composition of the mudrocks from the Moatize and Matinde formations is presented in Table 1.

The major elements geochemistry reflects the uniform mineralogical assemblages of mudrocks both formations. The Moatize mudrocks have average SiO_2, Al_2O_3, Fe_2O_3, and K_2O contents of 55.2 ± 4.1%, 22.9 ± 4.5%, 2.3 ± 2.3%, and 1.4 ± 0.4%, respectively (Table 1). The mean value of the K_2O/Al_2O_3 ratio (0.06 ± 0.03; Table 1) is lower than that of the Upper Continental Crust (UCC; 0.22; Taylor and McLennan, 1985) and Post Archean Australian Shales (PAAS; 0.20; Taylor and McLennan, 1985), but similar to values typical of clay minerals (<0.2; Cox et al., 1995).

The average Na_2O/K_2O ratio (0.08 ± 0.02) is also lower than that of the UCC (1.15; Taylor and McLennan, 1985) and PAAS (0.32; Taylor and McLennan, 1985). The average MnO (0.1 ± 0.1%), MgO (0.4 ± 0.2%), CaO (0.2 ± 0.1%), and Na_2O (0.1 ± 0.0%) contents are consistently very low (Table 1). The low CaO, Na_2O, and K_2O contents, together with their low correlation coefficients with Al_2O_3 (Table 2), suggest selective Ca, Na, and K leaching due to intense chemical weathering in the source area (see Discussion).

According to Herron (1988) classification, most Moatize Formation mudrocks plot within the shale field (Fig. 7), whereas two samples plot in the Fe-shales field or at the Fe-shales/Fe-sand boundary. Compared with UCC values, the Moatize Formation mudrocks exhibit similar SiO_2 contents, slightly higher TiO_2 and Al_2O_3 values, and are depleted in Fe_2O_3, MnO, MgO, CaO, Na_2O, K_2O, and P_2O_5 (Fig. 8a).

The Matinde Formation mudrocks exhibit a major element distribution pattern similar to that of the Moatize Formation, although with a slightly wider range in SiO_2, Fe_2O_3, and K_2O contents (Table 1). Their average SiO_2, Al_2O_3, Fe_2O_3, and K_2O contents are 56.6 ± 6.7%, 22.9 ± 4.0 %, 2.2 ± 3.8%, and 1.4 ± 0.7%, respectively. The MnO (0.03 ± 0.07%), MgO (0.3 ± 0.1%), CaO (0.2 ± 0.2%), and Na_2O (0.11 ± 0.05%) contents are also very low. Accordingly, the average of the SiO_2/Al_2O_3 (2.6 ± 0.6), K_2O/Al_2O_3 (0.07 ± 0.04), and Na_2O/K_2O (0.08 ± 0.02) ratios are comparable to those of the Moatize Formation mudrocks

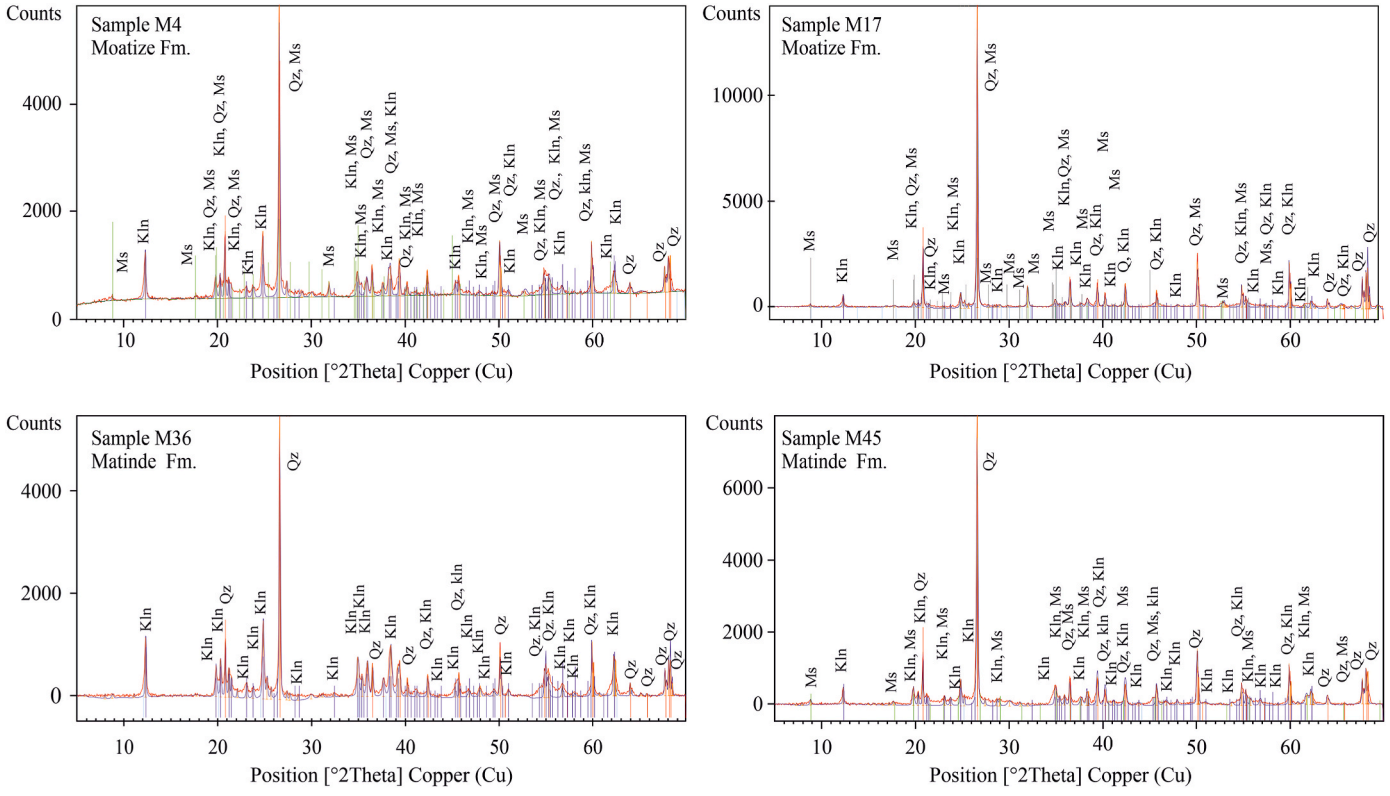

Fig. 6. XRD patterns showing clay and non-clay minerals in representative mudrocks from the Moatize and Matinde formations. Kln = kaolinite, Ms = muscovite, and Qz = quartz. (For interpretation of the references to colour in this figure legend, the reader is referred to the Web version of this article.)

Table 1
Average whole-rock composition of mudrocks of the Moatize and Matinde formations.

	Moatize Formation				Matinde Formation			
	n = 15	Std	Min.	Max.	n = 26	Std	Min.	Max.
Major elements (wt %)								
SiO_2	55.19	4.12	49.45	67.13	56.64	6.67	42.77	69.31
TiO_2	1.20	0.24	0.83	1.59	1.29	0.41	0.64	2.25
Al2O3	22.95	4.46	13.25	30.06	22.85	4.03	15.59	31.65
Fe_2O_3(T)	2.31	2.28	0.30	7.23	2.19	3.82	0.28	17.75
MnO	0.06	0.07	0.00	0.22	0.03	0.07	0.00	0.31
MgO	0.36	0.18	0.15	0.92	0.31	0.14	0.14	0.69
CaO	0.16	0.15	0.06	0.66	0.17	0.16	0.07	0.68
Na_2O	0.11	0.02	0.07	0.13	0.11	0.05	0.05	0.30
K_2O	1.40	0.41	0.66	2.07	1.38	0.66	0.60	3.72
P_2O_5	0.10	0.08	0.03	0.29	0.13	0.20	0.01	0.85
S	0.07	0.10	0.01	0.28	0.11	0.15	0.01	0.56
LOI	15.24	5.08	8.44	24.72	14.22	4.89	7.47	25.85
Total	99.15	0.70	98.20	100.58	99.42	0.70	98.53	100.63
Trace elements (ppm)								
Sc (ppm)	18.3	5.9	11.6	32.6	18.0	5.8	8.0	29.3
V	142.4	48.7	66.0	233.0	149.3	56.3	61.0	283.0
Cr	141.7	59.3	55.0	237.0	141.8	64.4	53.0	324.0
Co	17.3	15.2	1.0	44.0	14.8	23.3	1.0	102.0
Ni	42.7	24.6	14.0	85.0	44.9	70.3	11.0	375.0
Cu	48.7	15.8	21.0	74.0	47.9	19.5	14.0	96.0
Zn	105.8	55.5	33.0	220.0	118.3	127.7	20.0	606.0
Ga	33.3	5.1	23.0	42.0	35.5	8.0	23.0	55.0
Rb	82.9	16.1	48.0	108.0	84.8	41.9	35.0	232.0
Sr	211.9	219.3	70.0	937.0	313.2	576.8	31.0	2488.0
Y	35.4	8.6	21.2	48.4	36.5	8.4	19.4	53.8
Zr	239.5	71.9	164.0	396.0	260.8	76.5	124.0	443.0
Nb	22.3	5.2	15.4	34.0	23.3	6.8	12.7	38.6
Cs	7.4	2.3	3.0	11.3	7.5	3.1	3.3	14.7
Ba	589.4	499.8	203.0	2265.0	500.9	315.9	154.0	1480.0
Hf	5.9	1.5	4.1	8.6	6.4	1.8	3.1	11.4
Ta	1.9	0.4	1.4	2.7	2.0	0.6	1.0	3.4
Pb	25.5	11.4	11.0	51.0	27.6	18.0	4.0	91.0
Th	19.1	4.6	13.8	31.6	19.2	8.0	10.9	45.1
U	5.7	2.1	3.2	9.9	6.3	4.3	1.2	22.2
La	57.4	19.1	26.5	87.1	73.3	63.6	12.0	342.0
Ce	121.7	47.3	49.2	202.0	146.2	113.3	26.9	602.0
Pr	13.7	5.4	5.6	22.7	17.0	14.7	3.3	77.5
Nd	52.0	21.8	18.1	89.2	63.6	54.1	12.4	277.0
Sm	9.8	4.0	3.7	16.4	11.3	7.8	2.6	37.2
Eu	2.1	1.0	0.7	3.7	2.2	1.5	0.5	6.0
Gd	7.9	3.0	3.6	12.2	8.3	3.9	3.0	18.4
Tb	1.2	0.4	0.7	1.8	1.3	0.4	0.6	2.4
Dy	7.0	1.8	4.2	9.6	7.2	1.9	3.4	11.9
Ho	1.3	0.3	0.9	1.8	1.4	0.3	0.6	2.1
Er	3.7	0.8	2.5	5.0	3.8	0.9	1.8	5.7
Tm	0.5	0.1	0.4	0.7	0.5	0.1	0.3	0.8
Yb	3.5	0.7	2.4	4.6	3.5	0.7	1.9	4.8
Lu	0.5	0.1	0.3	0.7	0.5	0.1	0.3	0.7
K_2O/Al_2O_3	0.06	0.03	0.02	0.12	0.07	0.04	0.02	0.24
Na_2O/K_2O	0.08	0.02	0.04	0.13	0.08	0.02	0.04	0.12
Th/Sc	1.16	0.49	0.53	2.34	1.25	0.90	0.43	4.47
Cr/Th	7.85	4.01	3.14	15.70	8.28	4.46	3.31	21.35
La/Co	10.24	18.52	0.88	75.70	16.92	15.68	0.82	52.50
∑REE	282.24	102.10	124.19	430.92	340.16	258.05	74.47	1374.6
∑LREE	254.51	95.57	105.31	392.40	311.43	251.74	57.46	1335.70
∑HREE	25.66	6.57	16.21	34.83	26.48	7.54	12.28	46.80
Eu/Eu*	0.68	0.07	0.61	0.83	0.67	0.08	0.56	0.84
ICV	0.27	0.19	0.09	0.73	0.25	0.20	0.08	1.05
CIA	91.69	3.29	83.08	96.64	91.71	4.14	76.14	97.00
CIW	97.85	1.48	92.89	98.91	97.86	1.32	93.51	99.13

CIV = $[(Fe_2O_3+K_2O + Na_2O + CaO + MgO + MnO + TiO_2)/(Al2O_3]$ (Cox et al., 1995).
CIA = $[Al_2O_3/(Al_2O_3+CaO^*+Na_2O + K_2O)]x100$ (Nesbitt and Young, 1982).
CIW = $[Al_2O_3/(Al2O3+CaO^*+Na_2O)]x100$ (Harnois, 1988).

(Table 1). In Herron's (1988) discrimination diagram, most Matinde Formation mudrocks plot within the shale field, whereas some samples fall within the Fe-shales field or at the shale/wacke boundary (Fig. 7).

The UCC-normalised major element distribution patterns of the Matinde and Moatize mudrocks are similar, despite a slight decrease in MnO in the former. Compared with PAAS, the mudrocks from both formations exhibit lower contents of Fe_2O_3, MnO, MgO, CaO, Na_2O, and K_2O (Fig. 8a).

Table 2
Correlation matrix of geochemical data from mudrocks of the Moatize Formation.

	Al_2O_3	CaO	Na_2O	K_2O	V	Cr	Co	Ni
Al_2O_3	1							
CaO	−0.32	1						
Na_2O	0.13	−0.25	1					
K_2O	−0.39	0.52	0.19	1				
V	0.44	−0.23	0.60	−0.17	1			
Cr	0.56	−0.27	0.24	−0.26	0.792	1		
Co	0.04	0.01	0.06	0.38	0.259	0.29	1	
Ni	0.46	−0.20	0.44	0.07	0.484	0.38	0.72	1

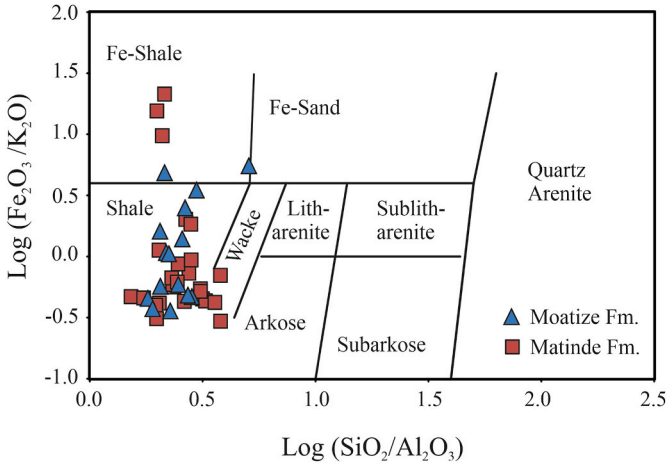

Fig. 7. Geochemical classification of the Moatize and Matinde mudrocks according to Herron (1988). (For interpretation of the references to colour in this figure legend, the reader is referred to the Web version of this article.)

4.3. Index of compositional variability

The mudrocks of the Moatize Formation exhibit ICV values ranging from 0.09 to 0.73, with an average of 0.27 ± 0.19. The mudrocks of the Matinde Formation have similar ICV values (0.08 – 1.05; mean 0.25 ± 0.20). The low ICV values in the mudrocks of both formations indicate high clay mineral contents (0.03 - 0.78; Cox et al., 1995) and reflect intense weathering in the source area and/or tectonically active settings (see Discussion).

4.4. Trace elements

Transition trace elements (TTE; Cr, V, Co, and Ni) generally exhibit similar behaviour during magmatic processes (Feng and Kerrich, 1990). To varying degrees, these metals can be affected by post-magmatic processes such as weathering, transport, and diagenesis (*e.g.,* McLennan et al., 1990; Bauluz et al., 2000; Augustsson et al., 2023). According to Hayashi et al. (1997), Cr, V, and Mo can be readily leached from source rocks during weathering under oxic conditions, become enriched in oxygenated seawater, and subsequently precipitate under reducing conditions (*e.g.,* in organic carbon-rich sediments).

The Moatize and Matinde mudrocks have average V, Cr, Co, and Ni contents similar to PAAS (150 ppm, 110 ppm, 23 ppm, and 55 ppm, respectively; Taylor and McLennan, 1985), despite a wide range of TTE contents, most pronounced in the Matinde samples (Table 1). In both formations, some samples (*e.g.,* M11, M12, M14, M23, M37, M51, and M52; see Electronic Appendix A) exhibit Cr contents higher than PAAS (>200 ppm). This Cr enrichment is not always accompanied by corresponding increases in Ni and V contents. Consequently, the Moatize and Matinde mudrocks exhibit wide Cr/Ni ranges (1.5 - 12.2 and 0.4 - 10.9, respectively). The same is true for Cr/V ratio (0.7 – 1.7 and 0.6 – 2.1, respectively).

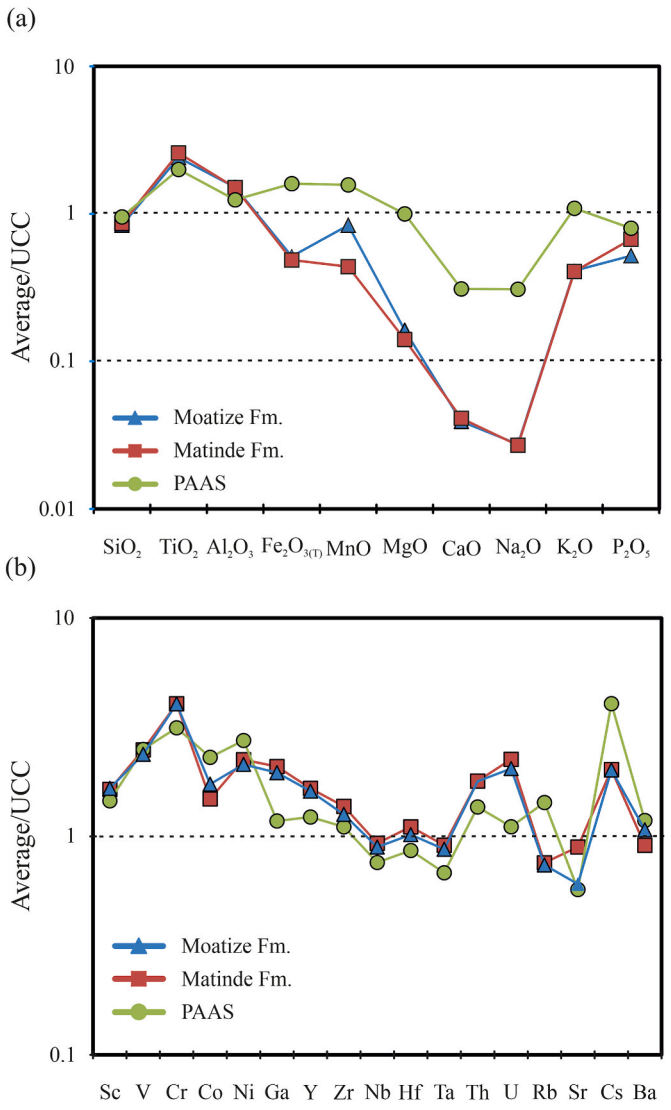

Fig. 8. (a) UCC-normalised average major and (b) trace elements composition of the Moatize and Matinde mudrocks. The plot of the Post-Archean Australian Shales (PAAS; Taylor and McLennan, 1985) is shown for comparison. Normalising values of UCC after Taylor and McLennan (1985). (For interpretation of the references to colour in this figure legend, the reader is referred to the Web version of this article.)

There is a moderate positive correlation between the Al_2O_3 contents and V (r = 0.44), Ni (r = 0.46), and Cr (r = 0.56) in the Moatize mudrocks (Table 2). In contrast, Cr shows weak correlations with Ni (r = 0.38) and Co (r = 0.29). In the Matinde mudrocks, Al_2O_3 contents show weak positive correlations with V (r = 0.13), Ni (r = 0.25), and Cr

Table 3
Correlation matrix of geochemical data from mudrocks of the Matinde Formation.

	Al_2O_3	CaO	Na_2O	K_2O	V	Cr	Co	Ni
Al_2O_3	1							
CaO	0.00	1						
Na_2O	−0.22	−0.11	1					
K_2O	−0.55	−0.14	0.80	1				
V	0.13	0.20	−0.02	−0.22	1			
Cr	0.19	−0.09	0.22	−0.02	0.56	1		
Co	0.13	0.09	0.17	−0.04	0.36	0.10	1	
Ni	0.25	−0.03	0.14	−0.06	0.16	0.10	0.90	1

(r = 0.19). Cr also exhibits weak positive correlations with Ni (r = 0.10) and Co (r = 0.10; Table 3).

In both sets of samples, Cr and V exhibit a moderately positive correlation (r = > 0.50; Tables 2 and 3). This correlation suggests that several mineral phases, such as clay minerals and accessory non-aluminous silicates, control TTE abundances in both formations. Compared with UCC values, the Moatize and Matinde mudrocks exhibit slight enrichment in Sc, V, Cr, Ni, and Co (Fig. 8b).

The mudrocks of the Moatize and Matinde formations exhibit wide Ba ranges (203 - 2265 ppm and 154 - 1480 ppm, respectively), although most samples are Ba-depleted relative to PAAS (650 ppm; Taylor and McLennan, 1985). A similar pattern is observed for the Sr in both formations (70 - 937 ppm and 31 - 2488 ppm, respectively). Compared with UCC values, the mudrocks of both formations exhibit variable depletions in Sr, Rb, and Ba (except for Ba in the Matinde Formation samples) and enrichment in Cs t (Fig. 8b).

High Field Strength Elements (HFSE; Th, Zr, Y, and Zr) are incompatible during igneous processes. As a result, these elements tend to be enriched in felsic relative to mafic sources (Feng and Kerrich, 1990; Asiedu et al., 2017). Compared to UCC, the mudrocks of both formations exhibit similar Nb and Ta contents but variable enrichments in Zr, Y, and Th. Additionally, the slight Zr enrichment observed in both formations suggests a limited influence of recycling processes during mudrock deposition (Fig. 8b).

The average Zr content of the Moatize and Matinde mudrocks is 240 ± 72 ppm and 261 ± 76 ppm, respectively. Both groups of mudrocks exhibit high correlation coefficients between Zr and Hf (r > 0.95), suggesting that zircon controls the abundance of these elements.

4.5. Rare earth elements

The Moatize and Matinde mudrocks have average total REE contents (∑REE) of 282 ± 102 ppm and 340 ± 258 ppm, respectively (Table 1). Samples from both formations show a wide range of light rare earth elements (LREE) concentrations (105 - 392 ppm and 57 - 1335 ppm, respectively), suggesting that LREE-bearing accessory minerals (*e.g.*, monazite, allanite, rutile) and/or quartz contents control the abundances of these elements.

Although the absolute REE concentrations are variable, the chondrite-normalised patterns of the Moatize and Matinde mudrocks are similar to those of the UCC, with distinctive LREE enrichment, nearly flat heavy rare earth elements (HREE) patterns, and a variable negative Eu/Eu* anomaly (Fig. 9). The Moatize mudrocks have average La_n/Sm_n (where n indicates chondrite normalisation), La_n/Yb_n, and Gb_n/Yb_n ratios of 3.9 ± 0.8, 11.3 ± 4.2 and 1.8 ± 0.6, respectively. The Matinde mudrocks exhibit similar values (4.1 ± 1.2, 13.8 ± 11.2, and 1.9 ± 1.0, respectively). In both formations, average Eu/Eu* values are similar (~0.67; see Table 1) and comparable to PAAS (0.66; Taylor and McLennan, 1985), and they do not vary systematically with stratigraphic height.

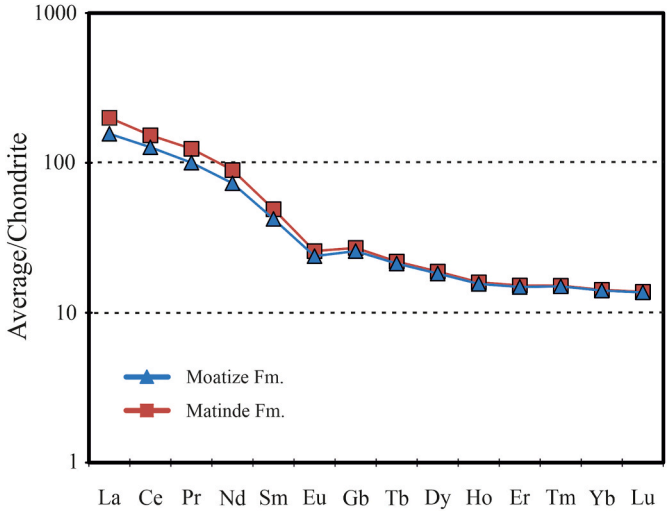

Fig. 9. Chondrite-normalised average REE patterns of the Moatize and Matinde mudrocks. Normalising values of chondrite after Taylor and McLennan (1985). (For interpretation of the references to colour in this figure legend, the reader is referred to the Web version of this article.)

4.6. Sr-Nd isotopic ratios

The Sr-Nd isotopic compositions of the mudrocks from both formations are presented in Table 4. The ε Nd (t), which represents the deviation of the $^{143}Nd/^{144}Nd$ ratio from a chondritic uniform reservoir (CHUR) and $f^{Sm/Nd}$, which measures the fractionation of Sm/Nd relative to CHUR, were calculated using the equations of DePaolo and Wasserburg (1976): $\varepsilon Nd\ (t) = [(^{143}Nd/^{144}Nd_{\ rock\ (t)})/(^{143}Nd/^{144}Nd_{\ CHUR(t)}) - 1] \times 10^4$ and $f^{Sm/Nd} = [(^{147}Sm/^{144}Nd_{\ rock)})/(^{147}Sm/^{144}Nd_{\ CHUR})\text{-}1]$, where $^{143}Nd/^{144}Nd_{\ CHUR} = 0.512636$ and $^{147}Sm/^{144}Nd_{\ CHUR} = 0.1967$. The initial $^{143}Nd/^{144}Nd_{(t)}$ ratios and $\varepsilon_{Nd(t)}$ values of the Moatize and Matinde mudrocks were calculated based on palynological ages of early Roadian (ca. 273 Ma) and of early Changhsingian (ca. 254 Ma), respectively (Lopes et al., 2014, 2021b; Pereira et al., 2014; Costa et al., 2016). Model ages were calculated assuming a depleted mantle (T_{DM}; DePaolo, 1981). Nd model ages were calculated as follows: $T_{DM} = 1/\lambda \ln [1 + ((^{143}Nd/^{144}Nd\ rock - {}^{143}Nd/^{144}Nd_{\ DM})/(^{147}Sm/^{144}Nd_{\ rock} - {}^{147}Sm/^{144}Nd_{\ DM}))]$; where $\lambda = 6.54 \times 10^{-12}\ a^{-1}$, $^{143}Nd/^{144}Nd_{\ DM} = 0.51315$ and $^{147}Sm/^{144}Nd_{\ DM} = 0.217$.

The measured $^{147}Sm/^{144}Nd$ ratios of mudrocks from the Moatize Formation range from 0.105 to 0.118 and εNd (0) values range from −10.10 to −11.82. The $f^{Sm/Nd}$ values vary between −0.40 and −0.47 (Table 4). The Matinde mudrocks have similar values for $^{147}Sm/^{144}Nd$ ratios (0.106 to 0.111), εNd (0) (−9.83 to −11.80) and $f^{Sm/Nd}$ (−0.43 to −0.46). The Nd T_{DM} model ages of the Moatize mudrocks range from 1.56 Ga to 1.79 Ga (1.68 ± 0.08 Ga), whereas those of the Matinde mudrocks range from 1.39 Ga to 1.63 Ga (1.51 ± 0.12 Ga).

The measured $^{86}Sr/^{87}Sr$ ratios of the Moatize mudrocks range from 0.7114 to 0.7260 (Table 4). The Matinde mudrocks exhibit a slightly higher range of $^{86}Sr/^{87}Sr$ ratios (0.7222 - 0.7235). The initial $^{86}Sr/^{87}Sr$ (t) ratios of the Moatize and Matinde formations vary from 0.7082 to 0.7125 and from 0.7117 to 0.7196 respectively. The Sr-isotopic signatures of both formations indicate a predominance of sediments derived from UCC.

5. Discussion

5.1. Sorting and sedimentary recycling

Hydrodynamic processes related to the transport and deposition of detrital grains can affect the distribution of the palaeoweathering and provenance proxies due to the influence of grain size contrasts, grain shape, and heavy mineral fractionation (*e.g.,* Bauluz et al., 2000; Garzanti et al., 2009; Augustsson et al., 2023). In siliciclastic sequences, zirconium and titanium are typically hosted in dense and ultra-dense minerals (zircon, rutile, and ilmenite) that are largely unaffected by chemical weathering, while titanium is also commonly hosted in Ti-bearing phyllosilicates (Fralick and Kronberg, 1997). The ternary Al_2O_3-TiO_2-Zr diagram minimises the effects of chemical weathering and reveals the extent of sorting-related fractionation processes (Garcia et al., 1991). This approach assumes that, during weathering and transport, the contents of insoluble elements may vary in response to the leaching of soluble elements but are transferred to the bulk sediment in proportion to their source area (Garcia et al., 1991, 1994). In this framework, mature sediments, characterised by sedimentary recycling, display a wide range of TiO_2/Zr and Al_2O_3/Zr ratios, whereas immature sediments exhibit a narrower range (Garcia et al., 1991, 1994; Mongelli

Table 4
Whole-rock Sr-Nd isotopic composition of the Moatize and Matinde mudrocks.

Sample	Sr (ppm)	Rb (ppm)	$^{87}Rb/^{86}Sr$	2σ	$^{87}Sr/^{86}Sr$	2σ	$^{87}Sr/^{86}Sr_{(t)}$ [a]	Nd (ppm)	Sm (ppm)	$^{147}Sm/^{144}Nd$	2σ	$^{143}Nd/^{144}Nd$	2σ	$f_{Sm/Nd}$ [b]	ε $Nd_{(0)}$ [c]	ε $Nd_{(t)}$	$T_{DM}(Ga)$ [d]
Moatize Formation																	
M4	242	101	1.208	0.034	0.717169	0.00003	0.712475	33	6.43	0.118	0.006	0.511981	0.000013	−0.40	−12.82	−10.07	1.79
M11	70	87	3.602	0.102	0.726038	0.000022	0.712046	38.1	6.6	0.105	0.006	0.512005	0.00002	−0.47	−12.35	−9.14	1.56
M15	284	82	0.836	0.024	0.711417	0.000021	0.708171	32.8	6.41	0.118	0.006	0.512069	0.000014	−0.40	−11.10	−8.36	1.66
M19	90	76	2.446	0.069	0.72149	0.000032	0.711988	71.9	13.7	0.115	0.003	0.511995	0.000018	−0.42	−12.54	−9.70	1.72
Matinde Formation																	
M27	186	70	1.09	0.031	0.723531	0.000032	0.719591	157	27.5	0.106	0.003	0.512134	0.00002	−0.46	−9.83	−6.89	1.39
M29	97	97	2.897	0.082	0.722166	0.000025	0.711697	84.5	15.8	0.113	0.003	0.512033	0.000022	−0.43	−11.80	−9.09	1.63

[a] t = 273 Ma (Moatize Formation) and 254 Ma (Matinde Formation).
[b] $f_{Sm/Nd} = [(147Sm/144Nd_{rock})/(147Sm/144Nd_{CHUR})-1]$, where $143Nd/144Nd_{CHUR} = 0.512636$ and $147Sm/144Nd_{CHUR} = 0.1967$.
[c] ε Nd (t) = $[(143Nd/144Nd_{rock}(t))/(143Nd/144Nd_{CHUR}(t)) - 1] \times 10^4$.
[d] $T_{DM} = 1/\lambda \ln(1+((143Nd/144Nd_{rock} - 143Nd/144Nd_{DM})/(147Sm/144Nd_{rock} - 147Sm/144Nd_{DM})))$; where $\lambda = 6.54 \times 10\text{-}12\ a^{-1}$, $143Nd/144Nd_{DM} = 0.51315$ and $147Sm/144Nd\ DM = 0.217$.

et al., 2006; Caracciolo et al., 2011; Al-Bassam et al., 2019). On the Al_2O_3-TiO_2-Zr diagram (Fig. 10a), the Moatize and Matinde mudrocks cluster in the centre, with a relatively constant TiO_2/Zr ratio, suggesting a limited influence of both sorting and recycling processes.

Zircon enrichment due to recycling can also be evaluated using Th/Sc versus Zr/Sc ratios (McLennan et al., 1990). Both ratios increase systematically during igneous differentiation, and no fractionation of these elements occurs during the sedimentary cycle. In first cycle sediments, Th/Sc and Zr/Sc ratios display a linear correlation controlled by the composition of the source rocks. In more mature or recycled rocks, Zr/Sc varies considerably due to zircon enrichment (*e.g.,* McLennan et al., 1990; Etemad-Saeed et al., 2011). The Th/Sc versus Zr/Sc diagram (Fig. 10b) shows that the mudrocks of both formations plot along or near this compositional trend, indicating limited variation in Zr/Sc ratios in all analysed samples. These results, suggest minimal sediment recycling and a low degree of sorting, possibly due to high sedimentation rates in an actively subsiding extensional basin (Key et al., 2015; Bicca et al., 2018; Lopes et al., 2021b). Furthermore, the immature character of the mudrocks indicates a sediment supply from proximal source area(s) throughout the Moatize and Matinde formations (Guadalupian to Lopinginan, middle to upper Permian). The occurrence of conglomerate beds of variable thickness (4 - 11 m) in the studied boreholes further supports the proximity of the sediment source areas. In the same area, conglomerates with similar sedimentary textures have been interpreted as the product of tectonic instability within the basin (Lopes et al., 2021b). At least until early Guadalupian times, the basement was exposed in the studied region as some conglomerates of that age rest unconformably on Precambrian basement rocks (Fernandes et al., 2023).

5.2. Source area(s) composition

It is widely accepted that REE, HFSE, and certain TTE (*e.g.,* Co, Sc, Cr, Ni) are particularly suitable for assessing the composition of source areas (*e.g.,* Taylor and McLennan, 1985; McLennan and Taylor, 1991). These elements are generally not fractionated during chemical or physical weathering, or during transport, have short residence times in the water column, and are transferred almost quantitatively to the sedimentary record (Wronkiewicz and Condie, 1987, 1990). Ratios between some of these compatible and incompatible elements are useful for distinguishing mafic from felsic source areas (*e.g.,* McLennan et al., 1990; Armstrong-Altrin et al., 2004; Asiedu et al., 2017).

The Moatize and Matinde mudrocks display similar REE normalised patterns, characterised by LREE enrichment and nearly flat HREE. The average La_n/Yb_n ratios in the Moatize and Matinde mudrocks are 11.3 ± 4.2 and 13.6 ± 10.9, respectively, values typical of siliciclastic rocks mainly derived from the UCC (Zimmermann and Spalletti, 2009). Taylor and McLennan (1985) and Wronkiewicz and Condie (1990) indicated that the Eu anomaly in fine-grained siliciclastic rocks is the most reliable fingerprint for assessing the geochemistry of the source area. Fine-grained sediments formed from the weathering of felsic rocks generally exhibit variable negative Eu anomalies, whereas sediments derived from mafic igneous rocks show small or no Eu anomalies (Cullers, 2000). In the Eu/Eu* versus Th/Sc diagram (Fig. 11a; McLennan et al., 1990; Slack et al., 2004), most Moatize and Matinde mudrocks plot within the fields of evolved felsic sources and, to a lesser extent, non-evolved felsic sources. A few Moatize and Matinde samples plot in mafic igneous source fields or along the boundary between felsic and mafic sources.

All samples were plotted on the La-Th-Sc diagram to assess the composition of the source area(s) of the Moatize and Matinde mudrocks (Fig. 11b; Wronkiewicz and Condie, 1987). In this diagram, most samples plot within the silicic rock field, between granitic and granodioritic sources, while a small number plot near the mafic rock field.

The Cr/Th ratio is also sensitive to the composition of the source area (*e.g.,* Wronkiewicz and Condie, 1990; Roddaz et al., 2007). Fine-grained

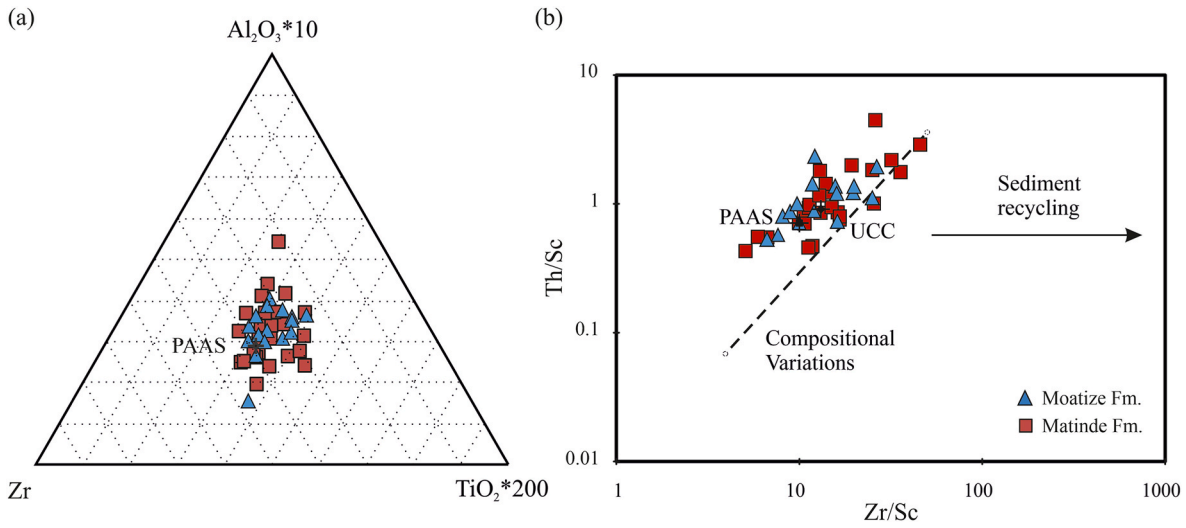

Fig. 10. (a) Zr-Al_2O3 (× 10)-TiO2 (× 200) diagram (after Garcia et al., 1994) for the mudrocks of the Moatize and Matinde formations. (b) Th/Sc v. Zr/Sc diagram (after Mclennan et al., 1990) shows that analysed mudrocks plot along or near the compositional trend, suggesting a limited influence of sediment recycling or sorting. (For interpretation of the references to colour in this figure legend, the reader is referred to the Web version of this article.)

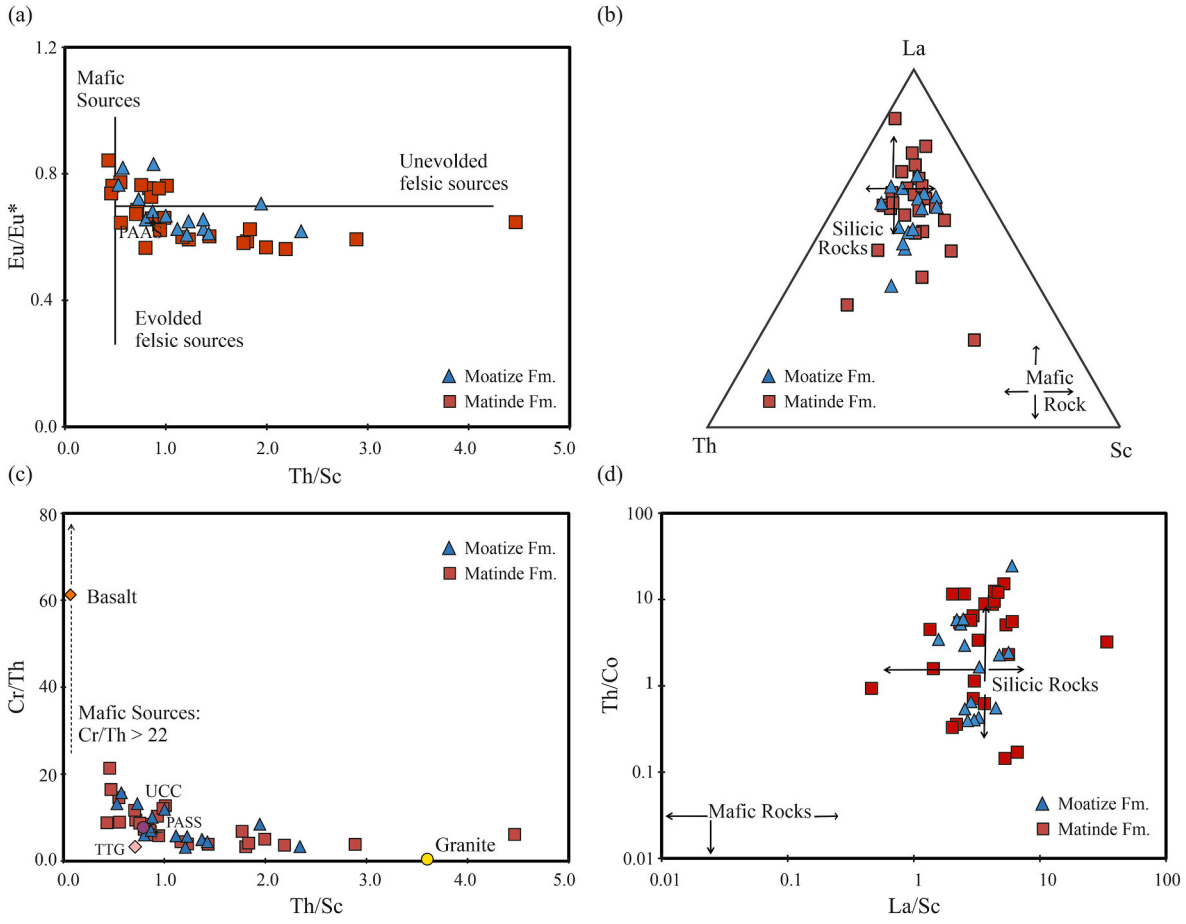

Fig. 11. Discrimination diagrams indicating sedimentary provenance: (a) Eu/Eu* versus Th/Sc (after Mclennan and Taylor, 1991; Cullers, 2000; Slack et al., 2004), (b) La-Th-Sc (after Wronkiewicz and Condie, 1987), (c) Cr/Th versus Th/Sc (after Coney et al., 2007) and (d) Th/Co versus La/Sc (after Cullers and Podkovyrov, 2002). (For interpretation of the references to colour in this figure legend, the reader is referred to the Web version of this article.)

sediments derived from felsic rocks typically exhibit Cr/Th ratios ranging from 0 to 15, whereas those derived from mafic rocks show higher values, between 22 and 500 (Cullers, 1994). The Moatize mudrocks have Cr/Th ratios ranging from 4.0 to 15.7, with an average 7.9 ± 4.0, only slightly lower than those of the Matinde Formation mudrocks (3.3 -21.4; 8.0 ± 4.4). In the Cr/Th versus Th/Sc diagram, most mudrocks of both formations plot within the granitic to granodioritic source field, with a group of samples clustering near the UCC and

PAAS compositions (Fig. 11c). The Th/Co versus La/Sc diagram (Cullers and Podkovyrov, 2002) also indicates a limited contribution from mafic sources (Fig. 11d).

The Nd isotopic system is a powerful tool for constraining the provenance of sediments and the tectonic setting of their depositional basins. The Nd T_{DM} of the siliciclastic rocks reflects the average crustal residence age of the catchment area(s) and the enables recognition of crustal domains of different ages and geological histories (*e.g.,* Arndt and Goldstein, 1987).

The ε Nd (t) values of the Moatize mudrocks range from −8.36 to −10.07 (−9.32 ± 0.74), whereas those of the Matinde mudrocks vary from −6.89 to −9.09 (−7.99 ± 1.56; Table 4). On the ε Nd (t) versus $f^{Sm/Nd}$ diagram, the Moatize Formation mudrocks plot on or near the boundary of the Early Precambrian Upper Crust (EPUCF) field (Fig. 12). The Matinde mudrocks exhibit a slightly different distribution pattern: one sample plots between the EPUC and the arc-rocks fields, suggesting the mixing of juvenile arc-derived material with sediments from an older crustal source.

Fig. 13 shows εNd(t) plotted against Nd T_{DM} for mudrocks from both formations, along with the potential source areas. Sm-Nd isotopic data for the study area are scarce, so the selection of potential source areas is supported by independent evidence: (a) sedimentological data and trace element systematics from the Matinde and Moatize mudrocks indicate sediment input from proximal source area(s); and (b) U-Pb geochronology of detrital zircons from the Matinde Formation reveals age spectra of ca. 1250-900 Ma, a secondary population between ca. 900-700 Ma, and a major contribution of ages around ca. 700-490 Ma (Bicca et al., 2018). These three main U-Pb age populations are interpreted as reflecting distinct source areas located to the south and east of the MMSB.

In Fig. 13, the distribution pattern of the analysed samples suggests a mixture of sources. Most samples from both formations cluster between the fields of the granitoids of SW Malawi - Nampula Block (a subdomain of southernmost Malawi) and the Guro Suite - Macossa - Chimoio Nappe. Some samples plot near the field of the Chewore-Rufunsa Terrane.

Additionally, average Nd T_{DM} values for the Moatize (1.68 ± 0.08 Ga) and Matinde (1.51 ± 0.12 Ga) formations are similar to those of the Guru Suite (1.65 ± 0.25 Ga) and to the granitoids of SW Malawi (1.41 ± 0.24 Ga; Fig. 14). The Sm-Nd isotopic signatures of mudrocks of both formations are consistent with U-Pb geochronological data (Bicca et al., 2018) and suggest sediment supply from the west-northwest to northwest (in present-day coordinates) during deposition of the Moatize and Matinde formations (Mugabe, 1999; Bicca et al., 2018; Fernandes et al., 2023).

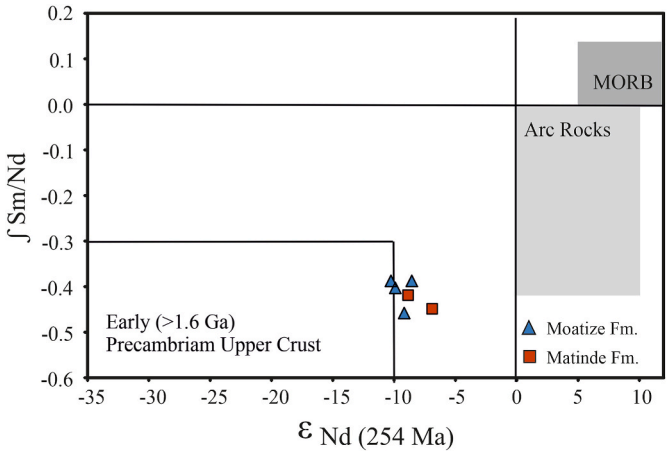

Fig. 12. ε Nd (t) versus $f^{Sm/Nd}$ plot for the Moatize and Matinde mudrocks. The fields of the Early Precambrian Upper Crust, Mid-Ocean Ridge basalt (MORB) and Island Arc Volcanic (Arc Rocks) are after Mclennan and Taylor (1991) and Mclennan et al. (1990). (For interpretation of the references to colour in this figure legend, the reader is referred to the Web version of this article.)

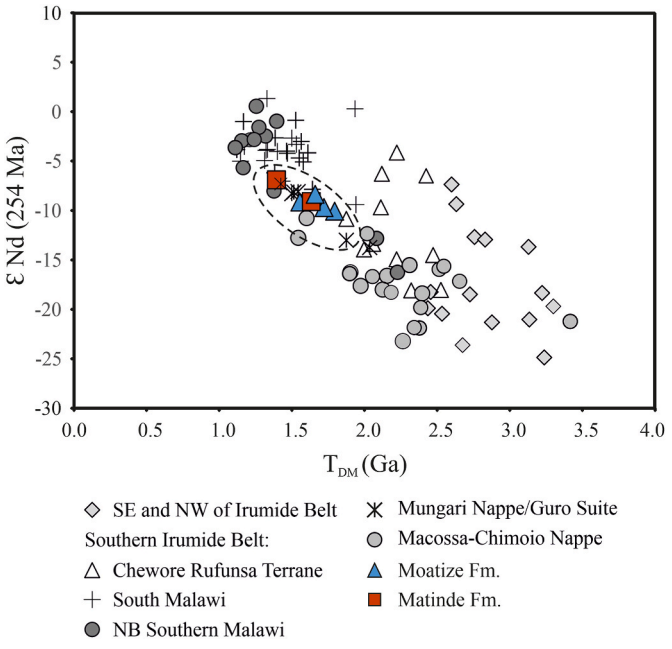

Fig. 13. εNd(t) versus Nd T_{DM} plot for the Moatize and Matinde formations mudrocks; whole-rock Sm-Nd data of the Zimbabwe Craton (Jelsma et al., 1996), SE and NE of the Irumide Belt (De Waele et al., 2006); Chewore Rufunsa Terrane (Johnson et al., 2007); South Malawi granitoids rock (Kroner et al., 2001; Manda et al., 2019) Nampula Block southern Malawi (Thomas et al., 2022) Mungari and Macossa-Chimoio Nappes (Grantham et al., 2011; Manjate, 2015; Manjate and Tasssinari, 2018) are included for comparison. The Nd T_{DM} values were calculated according to Stern (2002). (For interpretation of the references to colour in this figure legend, the reader is referred to the Web version of this article.)

5.3. Palaeoweathering conditions

The weathering of exposed UCC is dominated by the alteration of feldspars and the consequent formation of secondary clay and oxy-hydroxide minerals (Nesbitt and Young, 1982; Oliva et al., 1999; White and Blum, 1995; Ivory et al., 2014). Weathering rates and intensity strongly depend on temperature, pH, and total surface area, and are generally lowest at neutral pH (Drever and Clow, 1995). Intense weathering typically occurs in warm humid climates, whereas negligible weathering is characteristic of arid and cold climates (Nesbitt and Young, 1982; Lee et al., 2004).

Several multi-element weathering indices have been proposed based on the enrichment of immobile elements (*e.g.,* Al^{3+} and Ti^{4+}) and the depletion of mobile alkali and alkaline-earth cations (Ca^{2+}, K^{+}, Na^{+}, and Mg^{2+}) (*e.g.*, Parker, 1970; Harnois, 1988). Among these, the CIA (Nesbitt and Young, 1982) is widely used to assess source-area weathering and associated climatic conditions (*e.g.*, Young and Nesbitt, 1999; Wang et al., 2020).

The Moatize mudrocks exhibit CIA values between 83.1 and 96.6, with an average of 91.7 ± 3.3 (Fig. 15a). The Matinde mudrocks show similar CIA values ranging from 76.1 to 97.0 with an average of 91.7 ± 3.3 (Fig. 15b). Both formations have CIA values higher than PAAS (70 - 75; Taylor and McLennan, 1985, which is consistent with the low K/Cs ratios observed in most analysed samples (Fig. 16).

On the A–CN–K ternary diagram (Fedo et al., 1995), most samples plot subparallel to the A-K join and near the A apex (Fig. 15a and b). This distribution indicates that the mudrocks of both formations have not undergone post-depositional K-addition (*e.g.*, diagenetic illitisation and metasomatism).

The CIW can also quantify the degree of chemical weathering

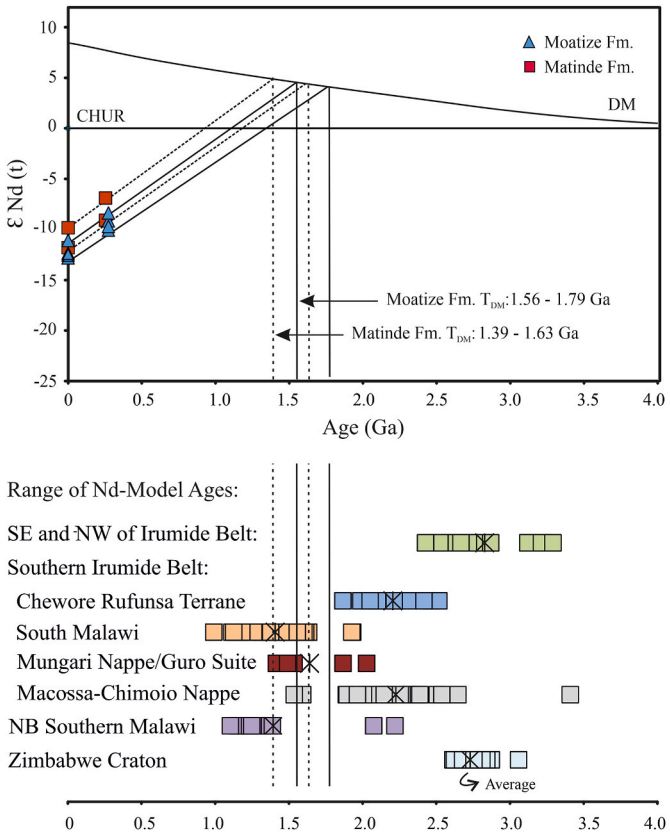

Fig. 14. εNd(t) versus Nd T_{DM} plot (after DePaolo, 1981) for the analysed mudrocks. Also plotted potential source areas of the Moatize and Matinde mudrocks (see legend of Fig. 13). DM = depleted Mantle; CHUR = chondritic uniform reservoir. (For interpretation of the references to colour in this figure legend, the reader is referred to the Web version of this article.)

(Harnois, 1988). The Moatize and Matinde mudrocks exhibit average CIW values of 97.8 ± 1.5 (92.9 - 98.8) and 97.9 ± 1.3 (93.5 - 99.1), respectively. The high CIW and CIA values of the fine-grained matrix of conglomerates from both formations (*e.g.*, samples M15, M5O, M51, and M29; see Electronic Appendix A) suggest a non-glaciogenic origin for these deposits, in agreement with sedimentological and palynological data (Caracciolo et al., 2011; Pereira et al., 2019; Lopes et al., 2021b). In glacial environments, low temperatures and limited moisture availability inhibit chemical weathering (*e.g.*, Hall et al., 2002; Wang et al., 2020). Accordingly, Permo-Carboniferous glacial sedimentary strata of the Dwyka Group from the MKB of South Africa have CIA values < 70, reflecting the predominance of physical over chemical weathering (Visser and Young, 1990; Huber et al., 2001; Scheffler et al., 2003; Gaschnig et al., 2014).

Altogether, the low ICV (<0.3) and high CIA and CIW values of the Moatize and Matinde mudrocks suggest that the source area(s) was subject to intense chemical weathering, reflecting warm and humid paleoclimatic conditions.

Well-documented post-glacial paleoclimatic reconstructions point to warm–humid conditions in the MKB of South Africa since the Early Permian (Scheffler et al., 2006). From the middle Permian to the

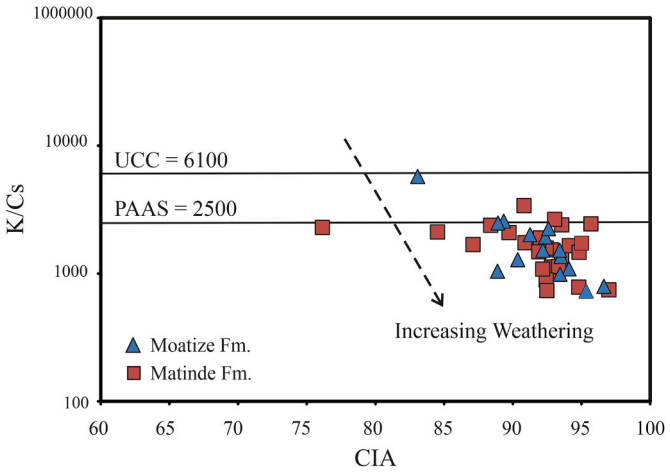

Fig. 16. K/Cs versus CIA plot (after McLennan et al., 1990) showing the weathering condition at the source area of the mudrocks of the MMSB. (For interpretation of the references to colour in this figure legend, the reader is referred to the Web version of this article.)

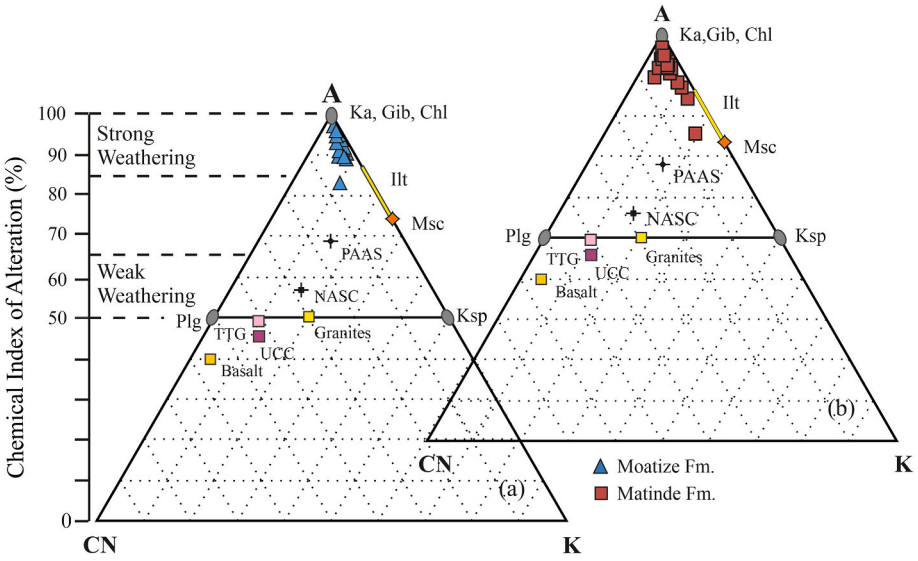

Fig. 15. A-CN-K diagrams (after Nesbitt and Young, 1982) for the Moatize (a) and Matinde (b) mudrocks. CIA = Chemical Index of Alteration; A = Al_2O_3; CN= CaO* + Na_2O; K= K_2O (molar proportions); CaO* is the amount of CaO incorporated in the silicate fraction of the sample; Pl = plagioclase; Ksp = K-feldspar; Ka = kaolinite; Gib = gibbsite; Chl = chlorite; Ms = muscovite; Ilt = Illite; TTG = Tonalite-trondhjemite-granodiorite. (For interpretation of the references to colour in this figure legend, the reader is referred to the Web version of this article.)

Triassic, increasing aridity inhibited the weathering, as indicated by decreasing CIA values over time (Scheffler et al., 2006; Geel and Bordy, 2021). Time-equivalent sedimentary successions in the Kalahari Basin show similar trends (Scheffler et al., 2006).

In contrast, the high CIA and CIW values of the Moatize and Matinde formations suggest distinct paleoclimatic and palaeoecological conditions in the Mid to Late Permian of the MMSB, compared to those reconstructed for the Main Karoo and Kalahari basins. These differences can be interpreted in two ways: (a) contrasting palaeolatitudes of the two groups of basins or, more likely, (b) the presence of a significant palaeotopographic barrier between the MMSB and the basins to the south (i.e., the Main Karoo and Kalahari basins), which generated unique paleoclimatic conditions.

Most palaeogeographic reconstructions indicate that a mountains chain, the Cargonian Highlands, lay between the MKB and the Karoo rift basins to the north (*e.g.,* Visser, 1987; Scheffler et al., 2006; Isbell et al., 2008; Pereira et al., 2019; Bordy, 2020). Similar highland areas may have persisted during the Middle to Late Permian, to the north of the rift basins, corresponding chiefly to Archean cratons and Precambrian orogens (Fig. 17). This palaeotopography may have favoured the preservation of local warm-humid conditions in the Karoo rift basins, as in the MMSB, where thick coal deposits accumulated the Mid to Late Permian.

The coal seams of the Moatize region are autochthonous coals formed in wet forest swamps with limited oxidation of the plant material (Vasconcelos, 1995). The thicknesses of these coal seams (*e.g.* over 30 m in the Chipanga Seam; Vasconcelos, 1995) and the stratigraphic distribution of the coal deposits, from the early Guadalupian to the latest Lopingian (Lopes et al., 2021a), attest to prolonged subsidence and the persistence of swamp-like conditions throughout this interval in the MMSB. The palynological assemblages from the studied boreholes also support this interpretation, indicating humid and warm climatic conditions that favoured abundant seed ferns (glossopterids) and gymnosperms (*e.g. Cordaites*), with associated ferns, sphenopsids, and lycopsids, typical of humid lowland environments (Lopes et al., 2021b; Pereira et al., 2019).

6. Conclusions

The mineralogy, whole-rock geochemistry, and Sr-Nd isotopic compositions of mudrocks from the Muarádzi Coalfield of the MMSD were systematically analysed, with a focus on the Moatize and Matinde formations. The findings support the following conclusions:

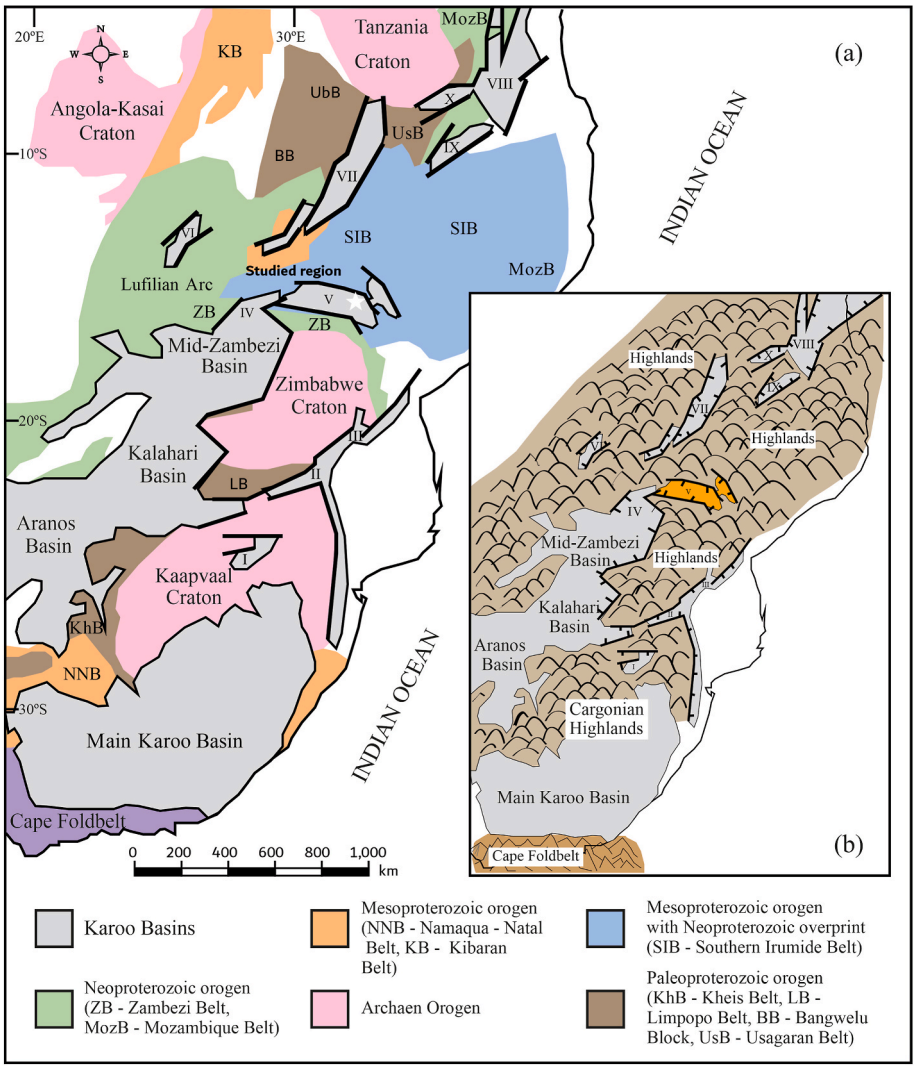

Fig. 17. (a) Distribution of the Karoo basins and the Precambrian terranes of southeast Africa. Adapted from Alessio et al. (2019). (b) Palaeogeography of Southeast Africa during Permian times, showing the intracontinental Karoo basins north of the Main Karoo Basin. I - Ellisras Basin, II - Tshipire Basin, III - Tuli, Save and Nuanetsi Basins, IV - Mana Pool Basin, V - Mozambique Zambezi River Valley Basins, VI - Barotse Basin, VII - Lukusashi and Luangwa Basins, VIII - Selous Basin, IX - Metangula Basin, X - Ruhuhu Basin. (For interpretation of the references to colour in this figure legend, the reader is referred to the Web version of this article.)

i) Both formations display similar mineralogical assemblages and comparable distribution patterns of major, trace, and REE elements, reflecting the combine influence of source area composition and weathering history;
ii) The geochemical signatures of the Moatize and Matinde mudrocks suggest a sediment supply from proximal source areas and a reduced influence of hydrodynamic sorting and recycling processes during mudstone deposition;
iii) REE patterns and key provenance proxies (*e.g.*, La/Sc, Th/Sc, Th/Co, and Cr/Th ratios) for both formations indicate sediment source areas dominated by felsic rocks, with a minor mafic contribution. The Sm-Nd isotopic record of the Moatize and Matinde formations further suggests that sediment supply was derived from mixed sources including late Mesoproterozoic and Neoproterozoic rocks of the Southern Malawi-Nampula Block (a subdomain of southernmost Malawi), the Guro Suite and the Macossa-Chimoio Nappe;
iv) The Moatize and Matinde mudrocks have high CIA and CIW values, as well as low K_2O/Al_2O_3 and K/Cs ratios. The high weathering indices of the fine-grained conglomerate matrix from both formations indicate a non-glaciogenic origin for these deposits. The CIA and CIW values for the analysed mudrocks suggest that the source areas of the Matinde and Moatize formations underwent intense chemical weathering, reflecting warm and humid paleoclimatic conditions. Additionally, these, data support palaeogeographic reconstructions that propose a palaeotopographic barrier between the MMSB and the southern Karoo-age basins;
v) The geochemical and isotopic data obtained in this study provide a better constraint on the paleoclimatic and paleogeographic evolution of the MMSD and other coal basins of similar age located north of MKB (*e.g.* the Ruhuhu and Selous basins in Tanzania) during the Middle to Upper Permian.

CRediT authorship contribution statement

P. Fernandes: Writing – review & editing, Writing – original draft, Investigation, Funding acquisition, Conceptualization. **Z. Pereira:** Writing – review & editing, Investigation. **J.F. Santos:** Writing – review & editing, Resources. **G. Lopes:** Writing – review & editing, Investigation. **J. Marques:** Writing – review & editing, Investigation.

Declaration of competing interest

There is no conflict of interests regarding this work.

No AI or AI-assisted technologies were used in the writing process of this manuscript.

Acknowledgements

This work was funded by the Portuguese Fundação para a Ciência e a Tecnologia (FCT) I.P./MCTES through national funds (PIDDAC) – UIDB/50019/2020, project PALEOCLIMOZ (PTDC/CTA-GEO/30082/2017), and projects LA/P/0069/2020, awarded to the Associate Laboratory ARNET, and UIDP/00350/2020, awarded to CIMA of the University of the Algarve. The authors would like to thank ETA STAR Moçambique, S. A. and Gondwana Empreendimentos e Consultorias, Limitada, for borehole access and complementary information. The anonymous reviewers are gratefully acknowledged for their valuable comments that improved the manuscript. PF and GL acknowledge the financial support of the FCT to CIMA under UID/00350/2020CIMA. RJ and PF acknowledge Manuel Francisco Pereira for access to the X-ray diffractometer, supported by FCT project UID/04028/2025. JFS thanks, also to FCT, the support through UIDB/04035/2020 (GeoBioTec).

Appendix B. Supplementary data

Supplementary data to this article can be found online at https://doi.org/10.1016/j.jafrearsci.2026.106106.

Data availability

Data will be made available on request.

References

Achimo, M., Vasconcelos, L., Marques, J., Ferrara, M., 2014. Sedimentologia dos depósitos tilíticos do vale do Rio Murrongódzi, Bacia Carbonífera de Moatize – minjova, Tete, Moçambique. In: 2° Congresso Nacional de Geologia e 12° Congresso de Geoquímica dos Países de Língua Portuguesa, pp. 57–61. Maputo, Moçambique.

Afonso, R.S., 1984. Ambiente geológico dos carvões gonduânicos de Moçambique - uma síntese. In: Lemos de Sousa, M.J. (Ed.), Symposium on Gondwana Coals, Lisbon, 1983. Proceedings and Papers, Comunicações dos Serviços Geológicos de Portugal, vol. 70, pp. 205–214.

Afonso, R.S., Marques, J.M., 1993. Recursos Minerais da República de Moçambique: Contribuição para o seu conhecimento. Instituto de Investigação Científica Tropical de Portugal, Centro de Geologia e Direcção Nacional de Geologia. Lisboa, Portugal.

Afonso, R.S., Marques, J.M., Ferrara, M., 1998. Evolução Geológica de Moçambique. Instituto de Investigação Científica Tropical de Portugal and Direcção Nacional de Geologia de Moçambique. Lisboa, Portugal.

Al-Bassam, K., Magna, T., Vodrázka, R., Cech, S., 2019. Mineralogy and geochemistry of marine glauconitic siliciclasts and phosphates in selected Cenomanian-Turonian units, Bohemian Cretaceous Basin, Czech Republic: implications for provenance and depositional environment. Geochemistry 79 (2), 347–368. https://doi.org/10.1016/j.chemer.2019.05.003.

Alessio, B.L., Collins, A.S., Siegfried, P., Gloriea, S., DeWaele, B., Paynee, J., Archibald, D.B., 2019. Neoproterozoic tectonic geography of the south-east Congo craton in Zambia as deduced from the age and composition of detrital zircons. Geosci. Front. 10 (6), 2045–2061. https://doi.org/10.1016/j.gsf.2018.07.005.

Armstrong-Altrin, J.S., Lee, Y.I., Verma, S.P., Ramasamy, S., 2004. Geochemistry of sandstones from the upper Miocene Kudankulam Formation, southern India: implications for provenance, weathering, and tectonic setting. J. Sediment. Res. 74, 285–297. https://doi.org/10.1306/082803740285.

Arndt, N.T., Goldstein, S.L., 1987. Use and abuse of crust-formation ages. Geology 15 (10), 893–895. https://doi.org/10.1130/0091-7613(1987)15<893:UAAOCA>2.0.CO;2.

Asiedu, D.K., Asong, S., Atta-Peters, D., Sakyi, P.A., Su, B.X., Dampare, S.B., Anani, C.Y., 2017. Geochemical and Nd-Isotopic compositions of juvenile type Paleoproterozoic Birimian sedimentary rocks from southeastern West African Craton (Ghana): constraints on provenance and tectonic setting. Precambr. Res. 300, 40–52. https://doi.org/10.1016/j.precamres.2017.07.035.

Augustsson, C., Aehnelt, M., Olivarius, M., Voigt, T., Gaupp, H., Hilse, U., 2023. Provenance from the geochemical composition of terrestrial clastic deposits — a review with case study from the intracontinental Permo-Triassic of European Pangea. Sediment. Geol. 456, 106496. https://doi.org/10.1016/j.sedgeo.2023.106496.

Baiyegunhi, C., Liu, K., 2021. Sedimentary facies, stratigraphy, and depositional environments of the Ecca Group, Karoo Supergroup in the Eastern Cape Province of South Africa. Open Geosci. 13, 748–781. https://doi.org/10.1515/geo-2020-0256.

Barbolini, N., Rubidge, B., Bamford, M.K., 2018. A new approach to biostratigraphy in the Karoo retroarc foreland system: utilising restricted-range palynomorphs and their first appearance datums for correlation. J. Afr. Earth Sci. 140, 114–133. https://doi.org/10.1016/j.jafrearsci.2017.11.031.

Bauluz, B., Mayayo, M.J., Fernandez-Nieto, C., Lopez, J.M.G., 2000. Geochemistry of Precambrian and Paleozoic siliciclastic rocks from the Iberian Range (NE Spain): implications for source-area weathering, sorting, provenance, and tectonic setting. Chem. Geol. 168, 135–150. https://doi.org/10.1016/S0009-2541(00)00192-3.

Bicca, M.M., Philipp, R.P., Jelinek, A.R., Ketzer, J.M.M., Scherer, C.M.D., Jamal, D.L., dos Reis, A.D., 2017. Permian-Early Triassic tectonics and stratigraphy of the Karoo Supergroup in northwestern Mozambique. J. Afr. Earth Sci. 130, 8–27. https://doi.org/10.1016/j.jafrearsci.2017.03.003.

Bicca, M.M., Jelinek, A.R., Philipp, R.P., Lana, C.C., Alkmim, A.R., 2018. Precambrian-Cambrian provenance of Matinde Formation, Karoo Supergroup, northwestern Mozambique, constrained from detrital zircon U-Pb age and Lu-Hf isotope data. J. Afr. Earth Sci. 138, 42–57. https://doi.org/10.1016/j.jafrearsci.2017.10.013.

Bordy, E.M., 2020. Depositional style changes during the Permo-Carboniferous-Early Jurassic evolution of the Central Kalahari Karoo Subbasin, Botswana. Geol. J. 55, 5514–5539. https://doi.org/10.1002/gj.3751.

Bordy, E.M., Paiva, F., 2021. Stratigraphic architecture of the Karoo river channels at the End-Capitanian. Front. Earth Sci. 8. https://doi.org/10.3389/feart.2020.521766.

Caracciolo, L., Le Pera, E., Muto, F., Perri, F., 2011. Sandstone petrology and mudstone geochemistry of the Peruc–Korycany Formation (Bohemian Cretaceous Basin, Czech Republic). Int. Geol. Rev. 53, 1003–1031. https://doi.org/10.1080/00206810903429011.

Catuneanu, O., Wopfner, H., Eriksson, P.G., Cairncross, B., Rubidge, B.S., Smith, R.M.H., Hancox, P.J., 2005. The Karoo basins of south-central Africa. J. Afr. Earth Sci. 43, 211–253. https://doi.org/10.1016/j.jafrearsci.2005.07.007.

Chaúque, F.R., Cordani, U.G., Jamal, D.L., Onoe, A.T., 2017. The Zimbabwe Craton in Mozambique: a brief review of its geochronological pattern and its relation to the Mozambique Belt. J. Afr. Earth Sci. 129, 366–379. https://doi.org/10.1016/j.jafrearsci.2017.01.021.

Chaúque, F.R., Cordani, U.G., Jamal, D.L., 2019. Geochronological systematics for the Chimoio-Macossa frontal nappe in central Mozambique: implications for the tectonic evolution of the southern part of the Mozambique belt. J. Afr. Earth Sci. 150, 47–67. https://doi.org/10.1016/j.jafrearsci.2018.10.013.

Coney, L., Reimold, W.U., Hancox, P.J., Mader, D., Koeberl, C., McDonald, I., Struck, U., Vajda, V., Kamo, S.L., 2007. Geochemical and mineralogical investigation of the Permian-Triassic boundary in the continental realm of the southern Karoo Basin, South Africa. Palaeoworld 16, 67–104. https://doi.org/10.1016/j.palwor.2007.05.003.

Costa, M., Castro, L., Fernandes, P., Pereira, Z., Marques, J., 2016. Palinostratigrafia e maturação orgânica do Karoo Inferior nas sondagens ETA 15 e ETA 71 da Bacia de Moatize-Minjova, província de Tete (Moçambique). Geonovas 29, 71–80.

Cox, R., Lowe, D.R., Cullers, R.L., 1995. The influence of sediment recycling and basement composition on evolution of mudrock chemistry in the southwestern United States. Geochem. Cosmochim. Acta 59, 2919–2940. https://doi.org/10.1016/0016-7037(95)00185-9.

Cullers, R.L., 1994. The chemical signature of source rocks in size fractions of Holocene stream sediment derived from metamorphic rocks in the Wet Mountains Region, Colorado, USA. Chem. Geol. 113, 327–343. https://doi.org/10.1016/0009-2541(94)90074-4.

Cullers, R.L., 2000. The geochemistry of shales, siltstones and sandstones of Pennsylvanian-Permian age, Colorado, USA: implications for provenance and metamorphic studies. Lithos 51, 181–203. https://doi.org/10.1016/S0024-4937(99)00063-8.

Cullers, R.L., Podkovyrov, V.N., 2002. The source and origin of terrigenous sedimentary rocks in the Mesoproterozoic Ui group, southeastern Russia. Precambr. Res. 117, 157–183. https://doi.org/10.1016/S0301-9268(02)00079-7.

Delvaux, D., 2001. Karoo rifting in Western Tanzania: precursor of Gondwana Break-up? Contribution to Geology and Palaeontology of Gondwana in Honour of Helmut Wopfner, pp. 111–125. Cologne, Germany.

DePaolo, D.J., 1981. Neodymium isotopes in the Colorado front range and crustal–mantle evolution in the Proterozoic. Nature 291, 193–196. https://doi.org/10.1038/291193a0.

DePaolo, D.J., Wasserburg, G.J., 1976. Nd isotopic variations and petrogenetic models. Geophys. Res. Lett. 3, 249–252. https://doi.org/10.1029/GL003i005p00249.

De Waele, B., Liegeois, J.P., Nemchin, A.A., Tembo, F., 2006. Isotopic and geochemical evidence of Proterozoic episodic crustal reworking within the Irumide Belt of southcentral Africa, the southern metacratonic boundary of an Archaean Bangweulu Craton. Precambr. Res. 148, 225–256. https://doi.org/10.1016/j.precamres.2006.05.006.

Drever, J.I., Clow, D.W., 1995. Weathering rates in catchments. Rev. Mineral. Geochem. 31, 463–484. https://doi.org/10.1515/9781501509650-012.

Etemad-Saeed, N., Hosseini-Barzi, M., Armstrong-Altrin, J.S., 2011. Petrography and geochemistry of clastic sedimentary rocks as evidences for provenance of the Lower Cambrian Lalun Formation, Posht-e-badam block, Central Iran. J. Afr. Earth Sci. 61 (2), 142–159. https://doi.org/10.1016/j.jafrearsci.2011.06.003.

Fedo, C.M., Nesbitt, H.W., Young, G.M., 1995. Unraveling the effects of potassium metasomatism in sedimentary rocks and paleosols, with implications for paleoweathering conditions and provenance. Geology 23, 921–924. https://doi.org/10.1130/0091-7613(1995)023<0921:UTEOPM>2.3.CO, 2.

Feng, R., Kerrich, R., 1990. Geochemistry of fine-grained clastic sediments in the archean Abitibi greenstone-belt, Canada: implications for provenance and tectonic setting. Geochem. Cosmochim. Acta 54, 1061–1081. https://doi.org/10.1016/0016-7037(90)90439-R.

Fernandes, P., Cogné, N., Chew, D.M., Rodrigues, B., Jorge, R.C.G.S., Marques, J., Jamal, D., Vasconcelos, L., 2015. The thermal history of the Karoo Moatize–Minjova Coal Basin, Tete Province, Mozambique: an integrated vitrinite reflectance and apatite fission-track thermochronology study. J. Afr. Earth Sci. 112, 55–72. https://doi.org/10.1016/j.jafrearsci.2015.09.009.

Fernandes, P., Hancox, P.J., Mendes, M., Pereira, Z., Lopes, G., Marques, J., Jorge, R.C.G.S., Albardeiro, L., 2023. The age and depositional environments of the lower Karoo Moatize Coalfield of Mozambique: insights into the postglacial history of central Gondwana. Palaeoworld. https://doi.org/10.1016/j.palwor.2023.07.001.

Fernandes, P., Jorge, R.C.G.S., Albardeiro, L., Chew, D., Drakou, F., Pereira, Z., Marques, J., 2024. Detrital zircon U-Pb geochronology of the Moatize and N'Condédzi coalfields, Zambezi Karoo Basin of Mozambique: implications for provenance, sediment dispersal and basin evolution. J. Afr. Earth Sci. 220, 105458. https://doi.org/10.1016/j.jafrearsci.2024.105458.

Fralick, P.W., Kronberg, B.I., 1997. Geochemical discrimination of clastic sedimentary rock sources. Sediment. Geol. 113, 111–124. https://doi.org/10.1016/S0037-0738(97)00049-3.

Fritz, H., Abdelsalam, M., Ali, k.a., Bingen, B., Collins, A.S., Fowler, A.R., Ghebreab, W., Hauzenberger, C.A., Johnson, P.R., Kusky, T.M., Macey, P., Muhongo, S., Stern, R.J., Viola, G., 2013. Orogen styles in the east African orogen: a review of the Neoproterozoic to cambrian tectonic evolution. J. Afr. Earth Sci. 86, 65–106. https://doi.org/10.1016/j.jafrearsci.2013.06.004.

Galasso, F., Pereira, Z., Fernandes, P., Spina, A., Marques, J., 2019. First record of Permo-Triassic palynomorphs of the N'Condedzi sub-basin, Moatize-Minjova Coal Basin, Karoo Supergroup, Mozambique. Rev. Micropaleontol. 64. https://doi.org/10.1016/j.revmic.2019.05.001.

Garcia, D., Coelho, J., Perrin, M., 1991. Fractionation between TiO_2 and Zr as a measure of sorting within shale and sandstone series (Northern Portugal). Eur. J. Mineral 3, 401–414.

Garcia, D., Fonteilles, M., Moutte, J., 1994. Sedimentary fractionations between Al, Ti, and Zr and the genesis of strongly peraluminous granites. J. Geol. 102 (4), 411–422. https://www.jstor.org/stable/30065660.

Garzanti, E., Ando, S., Vezzoli, G., 2009. Grain-size dependence of sediment composition and environmental bias in provenance studies. Earth Planet Sci. Lett. 277, 422–432. https://doi.org/10.1016/j.epsl.2008.11.007.

Gaschnig, R.M., Rudnick, R.L., McDonough, W.F., Kaufman, A.J., Hu, Z.C., Gao, S., 2014. Onset of oxidative weathering of continents recorded in the geochemistry of ancient glacial diamictites. Earth Planet Sci. Lett. 408, 87–99. https://doi.org/10.1016/j.epsl.2014.10.002.

Geel, C., Bordy, E.M., 2021. Palaeo-environmental and provenance reconstruction of the Lower Permian mudstones (lower Ecca Group) in the main Karoo Basin, South Africa. J. Afr. Earth Sci. 182. https://doi.org/10.1016/j.jafrearsci.2021.104303.

Götz, A.E., Hancox, P.J., Lloyd, A., 2020. Southwestern Gondwana's Permian climate amelioration recorded in coal-bearing deposits of the Moatize sub-basin (Mozambique). Palaeoworld 29, 426–438. https://doi.org/10.1016/j.palwor.2018.08.004.

Gradstein, F.M., Ogg, J.G., Schmitz, M.D., Ogg, G., ScienceDirect, 2020. Geologic Time Scale 2020. Elsevier, Amsterdam, Netherlands.

Grantham, G., Macey, P., Ingram, B., Roberts, M., Armstrong, R., Hokada, T., Shiraishi, K., Jackson, C., Bisnath, A., Manhica, V., 2008. Terrane correlation between Antarctica, Mozambique and Sri Lanka; comparison of geochronology, lithology, structure and metamrophism and possible implications for the geology of southern Africa and Antarctica. Geol.Soc. London, Special Publ. 308, 91–119. https://doi.org/10.1144/SP308.4.

Grantham, G.H., Manhica, A.D.S.T., Armstrong, R.A., Kruger, F.J., Loubser, M., 2011. New SHRIMP, Rb/Sr and Sm/Nd isotope and whole rock chemical data from central Mozambique and western Dronning Maud Land, Antarctica: implications for the nature of the eastern margin of the Kalahari Craton and the amalgamation of Gondwana. J. Afr. Earth Sci. 59, 74–100. https://doi.org/10.1016/j.jafrearsci.2010.08.005.

GTK-Consortium, 2006. Map Explanation, Sheets 1630–1634, 1732–1734, 1832–1834 and 1932–1934. Geology of Degree Sheets Mecumbura, Chioco, Tete, Tambara, Guro, Chemba, Manica, Catandica, Gorongosa, Rotanda, Chimoio and Beira, Mozambique., 2. Ministério dos Recursos Minerais, Direcção Nacional de Geologia, Maputo, 411pp. and 414 appendices.

Hall, K., Thorn, C.E., Matsuoka, N., Prick, A., 2002. Weathering in cold regions: some thoughts and perspectives. Prog. Phys. Geogr. Earth Environ. 26, 577–603. https://doi.org/10.1191/0309133302pp353ra.

Hancox, P.J., 2016. The coalfields of south-central Africa: a current perspective. Episodes 39 (2), 407–428. https://doi.org/10.18814/epiiugs/2016/v39i2/95785.

Harnois, L., 1988. The CIW index: a new chemical index of weathering. Sediment. Geol. 55, 319–322. https://doi.org/10.1016/0037-0738(88)90137-6.

Hartzer, F.J., Manhiça, V.J., Marques, J.M., Grantham, G., Cune, G.R., Feitio, P., Daudi, E.X.F., 2008. Carta Geológica de Moçambique na escala 1:1000000. Direcção Nacional De Geologia, Ministério dos Recursos Minerais, Maputo, Moçambique.

Hayashi, K., Fujisawa, H., Holland, H.D., Ohmoto, H., 1997. Geochemistry of similar to 1.9 Ga sedimentary rocks from northeastern Labrador, Canada. Geochem. Cosmochim. Acta 61, 4115–4137. https://doi.org/10.1016/S0016-7037(97)00214-7.

Herron, M.M., 1988. Geochemical classification of terrigenous sands and shales from core or log data. J. Sediment. Petrol. 58, 820–829. https://doi.org/10.1306/212F8E77-2B24-11D7-8648000102C1865D.

Huber, H., Koeberl, C., McDonald, I., Reimold, W.U., 2001. Geochemistry and petrology of Witwatersrand and Dwyka diamictites from South Africa: search for an extraterrestrial component. Geochem. Cosmochim. Acta 65, 2007–2016. https://doi.org/10.1016/S0016-7037(01)00569-5.

Isbell, J., Cole, D., Octavian, C., 2008. Carboniferous-Permian glaciation in the main Karoo Basin, South Africa: stratigraphy, depositional controls, and glacial dynamics. Spec. Pap. Geol. Soc. Am. 441, 71–82. https://doi.org/10.1130/2008.2441(05.

Ivory, S.J., McGlue, M.M., Ellis, G.S., Lezine, A.M., Cohen, A.S., Vincens, A., 2014. Vegetation controls on weathering intensity during the last deglacial transition in Southeast Africa. PLoS One 9 (11), e112855. https://doi.org/10.1371/journal.pone.0112855.

Jacobs, L., A, N., Winkler, D., Newman, K., Gomani, E., Deino, A., 2005. Therapsids from the Permian Chiweta beds and the age of the Karoo Supergroup in Malawi. Palaeontol. Electron. 8, 23p.

Jelsma, H.A., Vinyu, M.L., Wijbrans, J.R., Verdurmen, E.A.T., Valbracht, P.J., Davies, G.R., 1996. Constraints on Archaean crustal evolution of the Zimbabwe craton: a U- Pb zircon, Sm- Nd and Pb- Pb whole-rock isotope study. Contrib. Mineral. Petrol. 124, 55–70. https://doi.org/10.1007/s004100050173.

Johnson, M.R., Van Vuuren, C.J., Hegenberger, W.F., Key, R., Show, U., 1996. Stratigraphy of the Karoo Supergroup in Southern Africa: an overview. J. Afr. Earth Sci. 23, 3–15. https://doi.org/10.1016/S0899-5362(96)00048-6.

Johnson, S.P., De Waele, B., Tembo, F., Katongo, C., Tani, K., Chang, Q., Iizuka, T., Dunkley, D., 2007. Geochemistry, geochronology and isotopic evolution of the Chewore-Rufunsa terrane, southern Irumide Belt: a Mesoproterozoic Continental margin arc. J. Petrol. 48, 1411–1441. https://doi.org/10.1093/petrology/egm025.

Key, R.M., Cotterill, F.P.D., Moore, A.E., 2015. The Zambezi River: an archive of tectonic events linked to the amalgamation and disruption of Gondwana and subsequent evolution of the African plate. S. Afr. J. Geol. 118, 425–438. https://doi.org/10.2113/gssajg.118.4.425.

Kroner, A., Willner, A.P., Hegner, E., Jaeckel, P., Nemchin, A., 2001. Single zircon ages, PT evolution and Nd isotopic systematics of high-grade gneisses in southern Malawi and their bearing on the evolution of the Mozambique belt in southeast Africa. Precambr. Res. 109, 257–291. https://doi.org/10.1016/S0301-9268(01)00150-4.

Lee, Y.I., Lim, H.S., Yoon, H.I., 2004. Geochemistry of soils of King George Island, South Shetland Islands, West Antarctica: implications for pedogenesis in cold polar regions. Geochem. Cosmochim. Acta 68, 4319–4333. https://doi.org/10.1016/j.gca.2004.01.020.

Lopes, G., Pereira, Z., Fernandes, P., Marques, J., 2014. Datação Palinológica dos Sedimentos Glaciogénicos da Formação (Tilítica) de Vúzi, sondagem ETA 65, Bacia Carbonífera de Moatize-Minjova, Moçambique - Resultados Preliminares. In: Actas do IX Congresso Nacional de Geologia. 2° Congresso de Geologia dos Países de Língua Portuguesa, p. 100. Porto, Portugal.

Lopes, G., Pereira, Z., Fernandes, P., Marques, J., Mendes, M., Gotz, A.E., 2021a. Permian stratigraphy and palynology of the Lower Karoo Group in Mozambique - a 2020 perspective. Newsl. Stratigr. 54, 335–362. https://doi.org/10.1127/NOS/2021/0618.

Lopes, G., Pereira, Z., Fernandes, P., Mendes, M., Marques, J., Jorge, R.C.G.S., 2021b. Late Permian palaeoenvironmental evolution of the Matinde Formation in the Muaradzi Sub-basin, Moatize-Minjova Basin, Mozambique. J. Afr. Earth Sci. 176. https://doi.org/10.1016/j.jafrearsci.2021.104138Getrightsandcontent.

Macey, P.H., Thomas, R.J., Grantham, G.H., Ingram, B.A., Jacobs, J., Armstrong, R.A., Roberts, M.P., Hollick, L., Bingen, B., de Kock, G.S., Viola, G., Bauer, W., Gonzales, E., Bjerkgård, T., Henderson, I.H.C., Sandstad, J.S., Cronwright, M.S., Harley, S., Solli, A., Nordgulen, Ø., Motuza, G., Daudi, E., Manhica, V., 2010. Mesoproterozoic geology of the Nampula Subprovince, northern Mozambique: tracing fragments of Mesoproterozoic crust in the heart of Gondwana. Precambr. Res. 182, 124–148. https://doi.org/10.1016/j.precamres.2010.07.005.

Macey, P.H., Miller, J.A., Rowe, C.D., Grantham, G.H., Siegfried, P., Armstrong, R.A., Kemp, J., Bacalau, J., 2013. Geology of the Monapo klippe, NE Mozambique and its significance for assembly of central Gondwana. Precambr. Res. 233, 259–281. https://doi.org/10.1016/j.precamres.2013.03.012.

Manda, B.W.C., Cawood, P.A., Spencer, C.J., Prave, A., Robinson, R., Roberts, N.M.W., 2019. Evolution of the Mozambique Belt in Malawi constrained by granitoid U-Pb, Sm-Nd and Lu-Hf isotopic data. Gondwana Res. 68, 93–107. https://doi.org/10.1016/j.gr.2018.11.004.

Manjate, V.A., 2015. Caracterização geocronologica dos granitoides do Complexo de Barue e da Suite de Guro, centro-oeste de Moçambique: Implicações tectonicas e metalogenéticas. PhD Thesis, IGc/USP, São Paulo, 142pp. (unpubl.).

Manjate, V.A., Tasssinari, C.C.G., 2018. Zircon U-Pb chronology and Nd isotope systematics of the Guro Suite granitoids, Mozambique: implications for Neoproterozoic crust reworking events. J. Afr. Earth Sci. 148, 69–79. https://doi.org/10.1016/j.jafrearsci.2018.05.012.

Mclennan, S.M., Taylor, S.R., 1991. Sedimentary-rocks and crustal evolution: tectonic setting and secular trends. J. Geol. 99, 1–21. https://doi.org/10.1086/629470.

Mclennan, S.M., Taylor, S.R., Mcculloch, M.T., Maynard, J.B., 1990. Geochemical and Nd-Sr isotopic composition of deep-sea turbidites: crustal evolution and plate tectonic associations. Geochem. Cosmochim. Acta 54, 2015–2050. https://doi.org/10.1016/0016-7037(90)90269-Q.

Mongelli, G., Critelli, S., Perri, F., Sonnino, M., Perrone, V., 2006. Sedimentary recycling, provenance and paleoweathering from chemistry and mineralogy of Mesozoic continental redbed mudrocks, Peloritani mountains, southern Italy. Geochem. J. 40, 197–209. https://doi.org/10.2343/geochemj.40.197.

Mugabe, J.A., 1999. Karoo Deposits of Zambezi Graben - Moatize and Tete City Mozambique; Sedimentary Facies Distribution and Palynological Approach. University of Utrecht, Netherlands, p. 297.

Nesbitt, H.W., Young, G.M., 1982. Early Proterozoic climates and plate motions inferred from major element chemistry of lutites. Nature 299, 715–717. https://doi.org/10.1038/299715a0.

Norconsult-Consortium, 2007. Sheet Explanation, Report No. B6.f: Sheets 1039 Muidine, 1040 Palma, 1134 Ponta Messuli, 1135 Lupilichi, 1136 Milepa, 1137 Macalange, 1138 Negomano, 1139 Mueda, 1140 Mocímboa da Praia, 1234 Metangula, 1235 Macaloge-Chiconono, 1236 Ma- vago, 1237 Mecula, 1238 Xixano, 1239 Meluco, 1240 Quissanga-Pemba, 1334 Meponda, 1335 Lichinga, 1336 Majune, 1337 Marrupa, 1338 Namuno, 1339 Montepuez, 1340 Mecúfi, 1435 Mandimba, 1436 Cuamba, 1437 Malema, 1438 Ribáuè-Mecubúri, 1535 Insaca, 1536 Gurúè, 1635 Milange, 1636 Lugela-Mocuba, Geological Mapping – Lot 1. National Directorate of Geology, Ministry of Mineral Resources and Energy, Maputo, Mozambique.

Nyambe, I., Dixon, O., 2000. Sedimentology of the Madumabisa mudstone Formation (Late Permian), Lower Karoo Group, mid-Zambezi Valley Basin, southern Zambia. J. Afr. Earth Sci. 30, 535–553. https://doi.org/10.1016/S0899-5362(00)00037-3.

Oliva, P., Viers, J., Dupre, B., Fortune, J.P., Martin, F., Braun, J.J., Nahon, D., Robain, H., 1999. The effect of organic matter on chemical weathering: study of a small tropical watershed: Nsimi-Zoetele site, Cameroon. Geochem. Cosmochim. Acta 63, 4013–4035. https://doi.org/10.1016/S0016-7037(99)00306-3.

Parker, A., 1970. Index of weathering for silicate rocks. Geol. Mag. 107, 501–504. https://doi.org/10.1017/S0016756800058581.

Pereira, Z., Fernandes, P., Lopes, G., Marques, J., Vasconcelos, L., 2016. The Permian-Triassic transition in the Moatize-Minjova Basin, Karoo Supergroup, Mozambique: a palynological perspective. Rev. Palaeobot. Palynol. 226, 1–19. https://doi.org/10.1016/j.revpalbo.2015.12.001.

Pereira, Z., Fernandes, P., Lopes, G., Marques, J., Vaz, M., Costa, M., Correia, J., Castro, L., Galasso, F., 2019. Palynology of the Muaradzi sub-basin, Moatize-Minjova coal Basin, Karoo Supergroup, Mozambique. Rev. Palaeobot. Palynol. 269, 78–93. https://doi.org/10.1016/j.revpalbo.2019.06.006.

Pereira, Z., Lopes, G., Fernandes, P., Marques, J., 2014. Estudo palinoestratigráfico da sondagem ETA 72 do Karoo Inferior da Bacia de Moatize, Moçambique – Resultados Preliminares. Actas do IX Congresso Nacional de Geologia/2° Congresso de Geologia dos Países de Língua Portuguesa, p. 106. Porto, Portugal.

Phiri, C., Wang, P., Nyambe, I., 2016. Geology and potential hydrocarbon play system of Lower Karoo Group in the Maamba Coalfield Basin, southern Zambia. J. Afr. Earth Sci. 118. https://doi.org/10.1016/j.jafrearsci.2016.03.006.

Real, F., 1966. Geologia da Bacia do Rio Zambeze (Moçambique). Características geológico-mineiras da Bacia do rio Zambeze em território moçambicano. Junta de Investigações do Ultramar, Lisboa, Portugal, p. 183p.

Retallack, G.J., 2013. Permian and Triassic greenhouse crises. Gondwana Res. 24, 90–103. https://doi.org/10.1016/j.gr.2012.03.003.

Roddaz, M., Debat, P., Nikiéma, S., 2007. Geochemistry of Upper birimian sediments (major and trace elements and Nd–Sr isotopes) and implications for weathering and tectonic setting of the Late Paleoproterozoic crust. Precambr. Res. 159, 197–211. https://doi.org/10.1016/j.precamres.2007.06.008.

Rubidge, B.S., Day, M.O., 2020. Biostratigraphy of the Eodicynodon Assemblage Zone (Beaufort group, Karoo Supergroup), South Africa. S. Afr. J. Geol. 123, 141–148. https://doi.org/10.25131/sajg.123.0010.

Scheffler, K., Buehmann, D., Schwark, L., 2006. Analysis of late Palaeozoic glacial to postglacial sedimentary successions in South Africa by geochemical proxies - response to climate evolution and sedimentary environment. Palaeogeogr. Palaeoclimatol. Palaeoecol. 240, 184–203. https://doi.org/10.1016/j.palaeo.2006.03.059.

Scheffler, K., Hoernes, S., Schwark, L., 2003. Global changes during Carboniferous-Permian glaciation of Gondwana: linking polar and equatorial climate evolution by geochemical proxies. Geology 31, 605–608. https://doi.org/10.1130/0091-7613(2003)031<0605:GCDCGO>2.0.CO, 2.

Slack, J.F., Dumoulin, J.A., Schmidt, J.M., Young, L.E., Rombach, C.S., 2004. Paleozoic sedimentary rocks in the Red Dog zn-pb-ag district mid vicinity western Brooks Range, Alaska: provenance, deposition, and metallogenic significance. Econ. Geol. 99, 1385–1414. https://doi.org/10.2113/gsecongeo.99.7.1385.

Smith, R.M.H., 1990. A review of stratigraphy and sedimentary environments of the Karoo Basin of South Africa. J. Afr. Earth Sci. 10, 117–137. https://doi.org/10.1016/0899-5362(93)90164-L.

Stern, R.J., 2002. Crustal evolution in the East African Orogen: a neodymium isotopic perspective. J. Afr. Earth Sci. 34 (3–4), 109–117. https://doi.org/10.1016/S0899-5362(02)00012-X.

Taylor, S.R., McLennan, S.M., 1985. The Continental Crust: Its Composition and Evolution. Blackwell Scientific, Oxford, London, Edinburgh, Boston, Palo Alto, Melbourne.

Thomas, R.J., Fullgraf, T., Macey, P.H., Boger, S.D., Hölttä, P., Lach, P., Le Roux, P., Dombola, K., Zammit, C., 2022. The Mesoproterozoic Nampula Subdomain in southern Malawi: completing the story from Mozambique. J. Afr. Earth Sci. 196, 104667. https://doi.org/10.1016/j.jafrearsci.2022.104667.

Torsvik, T.H., Cocks, L.R.M., 2017. Earth History and Palaeogeography. Cambridge University Press, Cambridge.

Vasconcelos, L., 1995. Contribuição Para O Conhecimento Dos Carvões Da Bacia Carbonífera De Moatize, Província De Tete, República De Moçambique. Universidade do Porto, Porto, Portugal.

Vasconcelos, L., Achimo, M., 2010. O carvão em Moçambique. In: Cotelo Neiva, J.M., Ribeiro, A., Mendes Victor, L., Noronha, F., Ramalho, M.M. (Eds.), Ciências Geológicas – Ensino E Investigação Da Sua História. Geologia Das Ex-Colónias De África, pp. 191–206. Lisboa.

Viglietti, P.A., Rubidge, B.S., Smith, R.M.H., 2017. New late Permian tectonic model for South Africa's Karoo Basin: foreland tectonics and climate change before the end-permian crisis. Sci. Rep. 7, 10861. https://doi.org/10.1038/s41598-017-09853-3.

Viola, G., Henderson, I.H.C., Bingen, B., Thomas, R.J., Smethurst, M.A., de Azavedo, S., 2008. Growth and collapse of a deeply eroded orogen: insights from structural, geophysical, and geochronological constraints on the Pan-African evolution of NE Mozambique. Tectonics 27. https://doi.org/10.1029/2008TC002284.

Visser, J.N.J., 1987. The influence of topography on the permo-carboniferous glaciation in the Karoo Basin and adjoining areas, southern Africa. In: Washington DC American Geophysical Union Geophysical Monograph Series, 41, pp. 123–129. https://doi.org/10.1029/GM041p0123.

Visser, J.N.J., Young, G.M., 1990. Major element geochemistry and paleoclimatology of the Permo-Carboniferous Glacigene Dwyka Formation and Postglacial Mudrocks in southern Africa. Palaeogeogr. Palaeoclimatol. Palaeoecol. 81, 49–57. https://doi.org/10.1016/0031-0182(90)90039-A.

Wang, P., Du, Y., Yu, W., Algeo, T.J., Zhou, Q., Xu, Y., Qi, L., Yuan, L., Pan, W., 2020. The chemical index of alteration (CIA) as a proxy for climate change during glacial-interglacial transitions in Earth history. Earth Sci. Rev. 201, 103032. https://doi.org/10.1016/j.earscirev.2019.103032.

White, A.F., Blum, A.E., 1995. Effects of climate on chemical-weathering in watersheds. Geochem. Cosmochim. Acta 59, 1729–1747. https://doi.org/10.1016/0016-7037(95)00078-E.

Wronkiewicz, D.J., Condie, K.C., 1987. Geochemistry of Archean shales from the Witwatersrand supergroup, South-Africa: Source-Area weathering and provenance. Geochem. Cosmochim. Acta 51, 2401–2416. https://doi.org/10.1016/0016-7037(87)90293-6.

Wronkiewicz, D.J., Condie, K.C., 1990. Geochemistry and mineralogy of sediments from the Ventersdorp and Transvaal Supergroups, South-Africa: cratonic evolution during

the Early Proterozoic. Geochem. Cosmochim. Acta 54, 343–354. https://doi.org/10.1016/0016-7037(90)90323-D.

Young, G.M., Nesbitt, H.W., 1999. Paleoclimatology and provenance of the glaciogenic Gowganda Formation (Paleoproterozoic), Ontario, Canada: a chemostratigraphic approach. Geol. Soc. Am. Bull. 111, 264–274. https://doi.org/10.1130/0016-7606(1999)111<0264:PAPOTG>2.3.CO, 2.

Zimmermann, U., Spalletti, L.A., 2009. Provenance of the Lower Paleozoic Balcarce Formation (Tandilia System, Buenos Aires Province, Argentina): implications for paleogeographic reconstructions of SW Gondwana. Sediment. Geol. 219, 7–23. https://doi.org/10.1016/j.sedgeo.2009.02.002.